

Recognizing the need for improved blue scintillator tiles (for efficient optical match to green WLS materials), Bicron developed a blue variant of the above green fluors which exhibits higher efficiency than traditional ones and which also should be relatively rad-hard. More of this particular fluor will be made for use in further testing and tile manufacture.

A second blue variant, which should be more rad-hard, is planned.

Schedules for this work are included on the attached Bicron Rad-Hard Scintillator Program dated 18 August 1990.

#### SHEET PRODUCTION DEVELOPMENT

The sheet line has been totally torn down and refurbishment and rebuilding begun. The main structural frame has been sandblasted and repainted. The rolling drums have been stripped down and crated for transport to to a local company capable of performing the critical resurfacing. This represents approximately four man-weeks of labor and \$5K expenditure to date.

BICRON CORPORATION

Charles R. Hurlbut  
Manager, Organic Scintillators

SSC SUBSYSTEM  
RAD-HARD SCINTILLATOR PROGRAM

The following Scintillator development program will begin on Sept. 4, 1990 with Bicron manpower allocation as so indicated. The goal is to develop and demonstrate stable rad-hard plastic scintillator and WLS materials for sheet and fibers by Spring of 1991 providing time for iterative testing and reports submitted in late 1991. This work will build upon the foundation of knowledge in this field developed in the Bicron SBIR program.

A. CAST TILES FOR IMMEDIATE TESTING AND TOWER PROTOTYPE

All Variants on Type B (precursor to RH- mat'ls.)

Bases: PS, PVT, RH-4, RH-5

Quantities: 20-30 10 cm tiles each.

Shipment by:

Sept. 30, 1990

Recast one or two best physical types

50 tiles minimum

Shipment by:

Nov. 15, 1990

B. POLYMERS

RH-1:

Cease development work other than making a few more plates and fibers for testing purposes.

The manufacture of large amounts of this material was never intended. RH 1 served to prove a point: that our general approach to formulating rad-resistant polymers is likely correct. Furthermore, we have recently discovered a specific weakness in its chemical properties which additionally supports our original plan that the ultimate rad-hard polymers would be the RH-2 or RH-3 materials.

RH-2:

Based on chemical theory, this should be the most rad-hard scintillator base. Because of this, we will make a strong effort to solve a difficult polymerization problem.

Process development

- Cross-linking for sheet production  
feasibility trials completed

Sept. 30, 1990

Molecular weights

- High pressure polymerization  
feasibility trials completed

Oct. 15, 1990

Begin sheet casting trials

Oct. 1, 1990

Est. complete by

Feb. 28, 1991

Begin radiation trials

Jan. 5, 1991

Time commitment: 33% of full time basis

Wayne Moser

RH-3:

- Priority over RH-2
- Monomer synthesis, 1/2 liter initially,  
2 weeks full-time, starting with new lab,  
Complete date: (5-6 wks. calendar time) Oct. 15, 1990  
Wayne Moser and Bill Harder
- Trial ampules  
Pure and Type B fluor formula  
Molecular weights  
First small ampule samples out on Nov. 11, 1990
- Begin R&D preform casting trials Nov. 20, 1990
- Begin sheet casting trials Dec. 1, 1990  
Est. complete by Feb. 28, 1991
- Begin radiation testing Jan. 5, 1991

C. FLUORS

Bicron Synthesis Research

Work up lab-scale preps for our continued supply and leading to large scale manufacture.

Bill Harder: 3 man-months = 6 calendar months

- Delta and Epsilon, First Priority
- Beta and Gamma
- V-2 and V-3  
Perhaps V-4 and V-5, coordinate with PCPS work
- P-2 and P-3

Characterization

Photophysics:

Dilute and concentrated in toluene

Concentrated in PS

Light output, solutions and plastic scints.

Decay times of plastics

Wayne Moser: complete by Nov. 30, 1990

Fiber preforms of best, starting Dec. 1, 1990

Update selection at that time

Radiation studies starting Jan. 15, 1991

D. FLUOR DEVELOPMENT AT PHILA. COLLEGE OF PHARMACY

Primary Task: Develop efficient, high Stokes-loss, fast waveshifter fluors with following

shifting spectra:	<u>Absorption</u>	<u>Emission</u>
	430-460 nm	500-550 nm
	430-460 nm	580-620 nm
	450-500 nm	580-620 nm

Secondary Task: Rad-hard monomer research:

Date complete: Jan. 31, 1991

E. INDUSTRIAL FLUORS STUDY

Photophysics

Approximately six fluors, green and red

Absorbance: dilute and conc. in toluene

Emission:

As function of concentration in toluene

Front and backface spectra

In PS at 100 mg/l.

Wayne Moser: two man-weeks, complete

Nov. 30, 1990

BICRON CORPORATION

C. Hurlbut

18 August 1990

### CONCLUSIONS

The first key issue for a calorimeter based on plastic scintillator for an SSC experiment is that of radiation damage. For a calorimeter based on scintillator to be at all viable, it is essential to demonstrate the survivability of plastic scintillator in the expected radiation field at the SSC (of order 1 to 10 MRad over most of the central rapidity region). Initial tests of both blue scintillator plates and assorted fibers show that at the component level, significant progress has been made in this area this year. For example after 1 MRad of irradiation followed by 22 days of annealing, a scintillator plate based on the Bicron RH1 plastic showed no measurable change in either attenuation length or initial light output (within a 1% measurement error). Similarly, a fiber based on the green scintillator 3HF showed only a 10% decrease in attenuation length and an 8% loss in light output after an irradiation of 3 MRad followed by a few days of annealing. These successes coupled with the fact that scintillator manufacturers are bettering their understanding of the damage and recovery process and thereby hope to significantly improve on this performance demands that we continue to aggressively pursue this approach to calorimetry at the SSC. We are therefore so proposing in our FY91 plan and in addition intend to acquire a deeper understanding of the system dependent issues of radiation damage on the performance of the calorimeter.

The choice of absorber is the second key issue for our design of calorimeter as our stated goal is a compensating calorimeter with high precision and uniformity. Our simulation studies have shown that both depleted uranium and lead absorbers of appropriate thicknesses relative to the chosen thickness of the scintillator plate can yield a calorimeter which has equal response to

both hadrons and electrons or photons of the same energy. A calorimeter based on a pure iron absorber does not. In addition, the time dependence of compensation in both lead and depleted uranium systems is very similar in the initial part of the shower and both can yield a response which is almost compensating in less than the 16 nsec between bunches at the SSC ( $e/h < 1.05$ ). Therefore, even trigger signals for these calorimeters measure an essentially compensating response. Energy release from delayed de-excitation of neutron capture reactions is observed only in the uranium system and may be the physics reason to prefer lead. This gives approximately 3-10% of the total signal stretching out over 200-500 nsec. Although we have not yet quantified the experimental effect of this energy, such pileup is very undesirable (and yet more so at the higher potential luminosities). Mechanical solutions for both choices of absorber have been evaluated using both analytical and simulation techniques. Both absorbers are feasible with the caveats that both allow azimuthal load transfer in the body of the calorimeter and that in the case of lead it is embedded in a composite structure. This structure is estimated to comprise at worst  $< 10\%$  of the lead volume and potentially can be distributed where it will have least affect on the performance of the calorimeter (this is part of the work being proposed for FY91). Moreover, the fabrication process of lead casting and the cost of the raw material greatly favours lead over depleted uranium. It is therefore our assessment that the appropriate choice for the absorber is lead and lead/composite and that the fabrication process to be used should be casting. Our proposal of work for FY91 assumes this conclusion and is directed at demonstrating this conclusion with physical devices.

Two options for the optical system used to couple scintillation light from the plate to the photon transducer were conceptually evaluated. Wavelength shifter plate is a very well known and well understood approach and for it. One the serious limitation for waveshifter plate is in the necessity to allow azimuthal load transfer between modules and therefore the need to modify the plate cross section at these radii (with resulting serious implications for both lateral and depth uniformity). A second serious limitation is the dead fiducial volume associated with the waveshifter plate and its associated air gaps and tolerances to preclude its being crushed. This loss can amount to as much as 7% of the surface area and although energy measurement in this region can be obtained by a suitable tilting of the front section, high quality electron measurements in this region would probably be impossible. The third serious limitation of this approach is Cerenkov light in the waveshifter plate itself. Although this can again be largely removed by tilting the front section of the calorimeter, this design, by using single sided readout to reduce dead space, has no intrinsic capability of identifying such light and thereby of vetoing the associated spurious signals. On the other hand, readout via embedded wavelength shifting fibers can potentially remove all of these limitations and in addition could be used in a design to allow refurbishment of those parts of the calorimeter exposed to the greatest radiation damage. However, it has a very large potential for intrinsic non-uniformity. The Fermilab group lead by G. W. Foster and J. Freeman have completed some early tests using this optical approach and have had considerable success. It is our assessment that this approach is the one with greatest potential for achieving our stated goal of maximum hermeticity and fiducial volume and we therefore propose it, as the favoured choice, as the one to be allocated our resources in FY91. It is nonetheless true that should we demonstrate that scintillator itself is radiation hard, then should we fail

to accomplish the necessary performance with a fiber-based readout then waveshifter plate can also be accommodated within this mechanical design (albeit with reduced performance of the calorimeter relative to our goals).

As a result of conclusions we opened discussions with the fiber tile component of the scintillating-fiber group with regard to a combined proposal in FY91. These discussions concluded with an agreement to submit a combined proposal in FY91 to specifically develop a calorimeter based on scintillator tile with embedded wavelength shifter fiber readout. Our main point of contention is that they anticipate that an iron based calorimeter with tuned absorber inserts can yield adequate compensation whereas we anticipate that a lead/composite structure (in which the composite is also iron) can be designed to be mechanically stable and to yield adequate compensation. All other areas of development are common to both absorber choices. Whether this calorimeter is eventually described as iron with some lead to achieve compensation or lead with some iron to yield mechanical stability is one of the key issues to be resolved by this collaboration in FY91.

## APPENDIX I

### Report on Benchmarking CALOR at ANL

*Job.P.K., Jim Proudfoot and Larry Price*

The Benchmarking of CALOR 89 for two scintillator plate systems has been carried out at Argonne. The salient features of the three systems chosen for benchmarking are given in table I. Out of this Iron and Lead systems were analysed at ANL.

All calculations were done for 10 GeV pions and electrons. The energy cut used for hadrons in HETC is 1.0 MeV. The energy cut used for electrons in EGS is 1.5 MeV and for photons 0.1 MeV. The ESTEPE parameter in EGS is not used. Neutrons below 20 MeV were transported by MORSE. The low energy photons from EGS were not transported by MORSE because of their negligible effect on the energy deposition ( less than 0.2% ). The light curves were calculated for Birks Constant 0.0131 and were used in SPECT and MORSE.

The electron response plot, longitudinal shower distribution and two dimensional shower distribution were calculated using EGS on a CRAY-XMP. The CALOR suite of codes were run on an IBM 3084. The eventwise energy deposition in the scintillator plates from each of the three codes of CALOR (HETC, EGS and MORSE) and their averages were calculated and stored in separate files. From these files the response plot for pions were calculated by a user written program.

Table II gives the summary results. The response plots for pions and electrons, their resolutions and the e/h ratio for both the configurations are given. These values are to be verified independently by the other groups.

TABLE I  
SALIENT FEATURES OF BENCHMARK CONFIGURATIONS

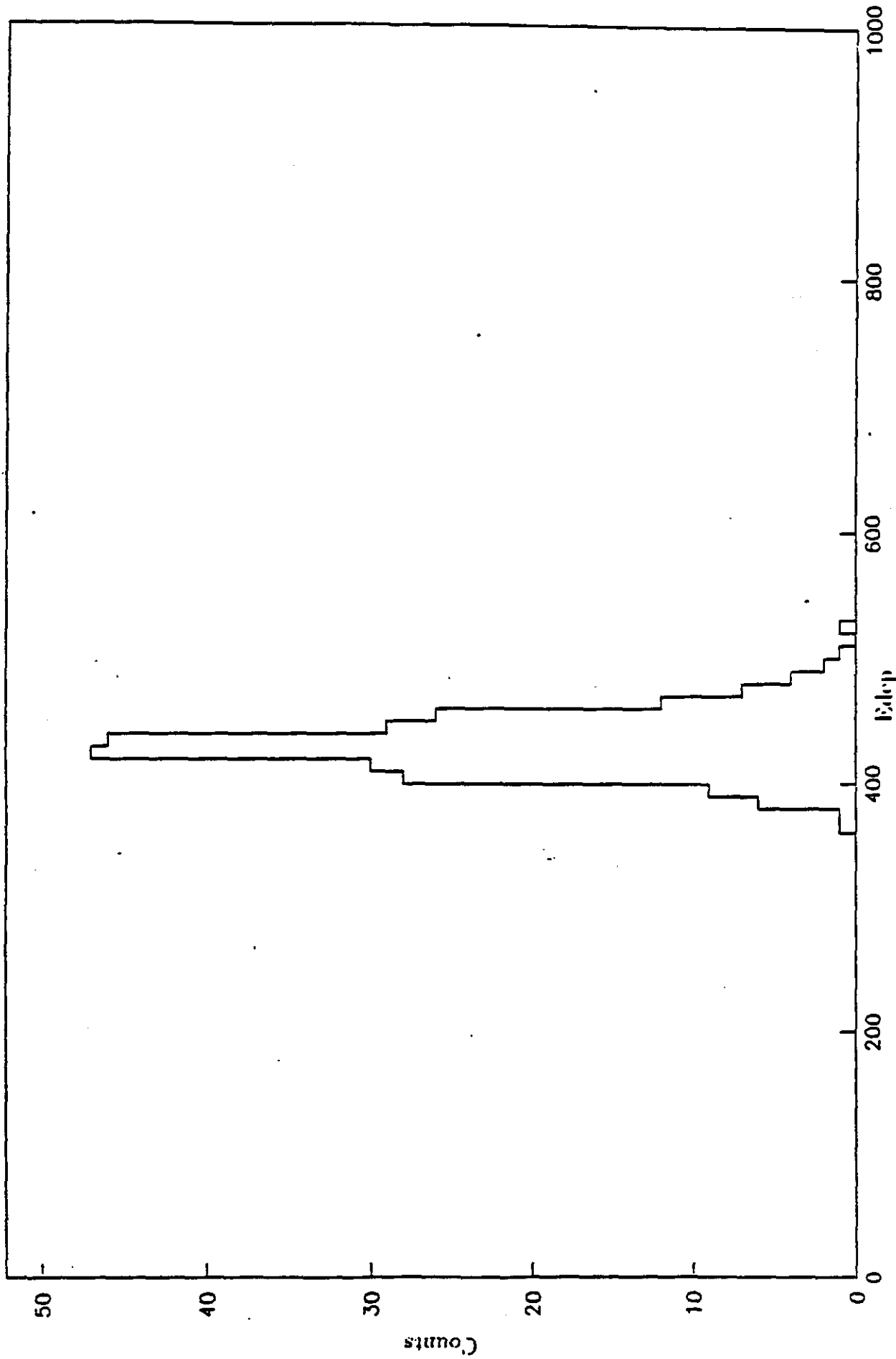
	DU-SCIN	Pb-SCIN	Fe-SCIN
Absorber medium	Depl. Uranium	Lead	Iron
Absorber Thickness	0.33 cm	0.56 cm	1.76 cm
Radiation Length	0.33 cm	0.56 cm	1.76 cm
Nuclear Int. length	10.5 cm	16.76 cm	17.09 cm
Density	18.95 gm/cm <sup>3</sup>	11.35 gm/cm <sup>3</sup>	7.87 gm/cm <sup>3</sup>
Number Density	4.794*10 <sup>22</sup>	3.299*10 <sup>22</sup>	8.486*10 <sup>22</sup>
Active medium	Scintillator	Scintillator	Scintillator
Scintillator Thickness	0.25 cm	0.25 cm	0.25 cm
Density	1.04 gm/cm <sup>3</sup>	1.04 gm/cm <sup>3</sup>	1.04 gm/cm <sup>3</sup>
Number Density			
Carbon	4.81*10 <sup>22</sup>	4.81*10 <sup>22</sup>	4.81*10 <sup>22</sup>
Hydrogen	4.92*10 <sup>22</sup>	4.92*10 <sup>22</sup>	4.92*10 <sup>22</sup>
Birks Constant	0.0131	0.0131	0.0131
Global Dimensions	100*100 cm <sup>2</sup>	100*100 cm <sup>2</sup>	100*100 cm <sup>2</sup>
Depth	8 $\lambda_{int}$	8 $\lambda_{int}$	8 $\lambda_{int}$

Table I

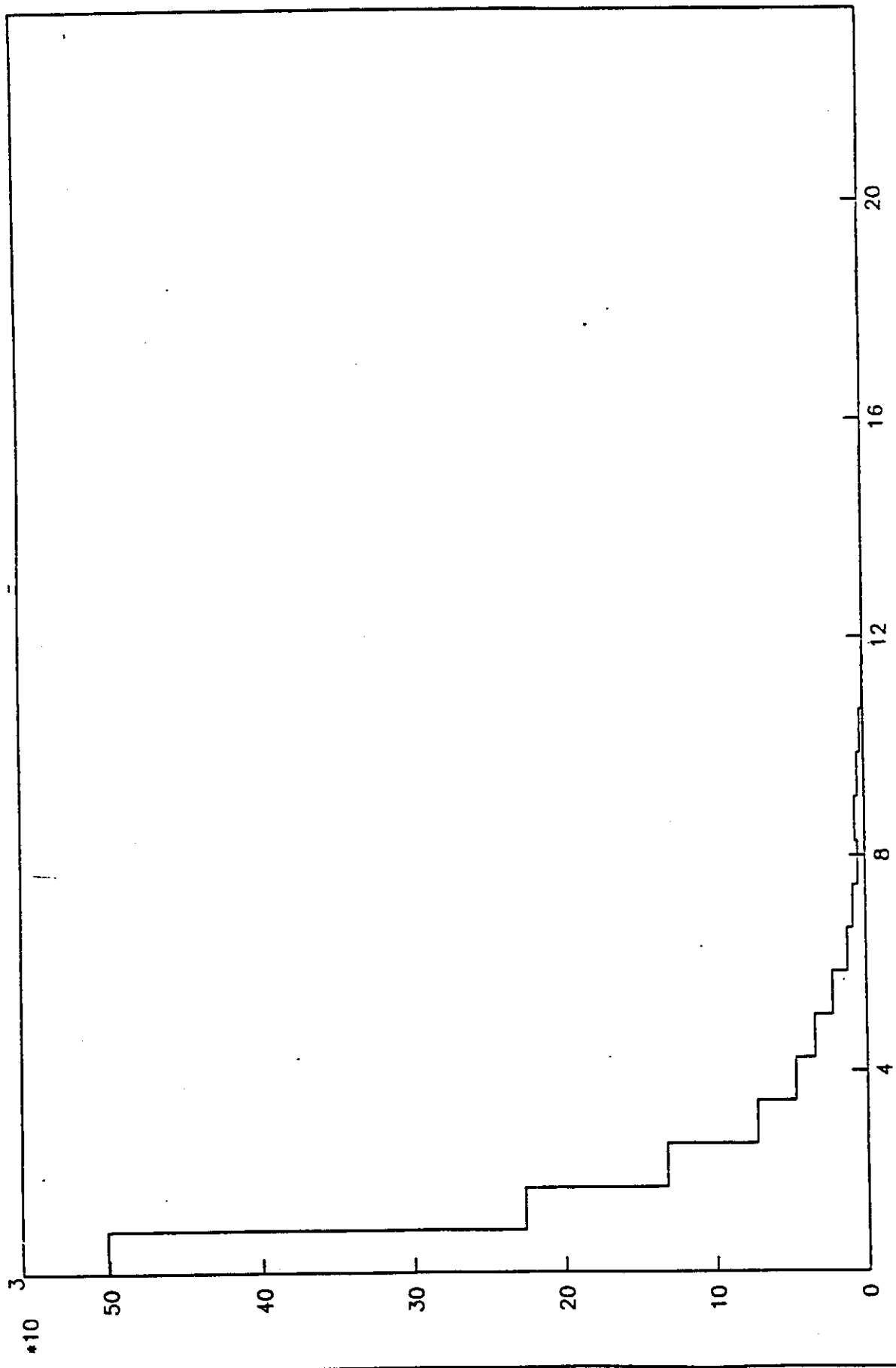
Energy Deposition in Scintillator (MeV)

(For 10 GeV Incident Energy and 50 nsec Integration Time)

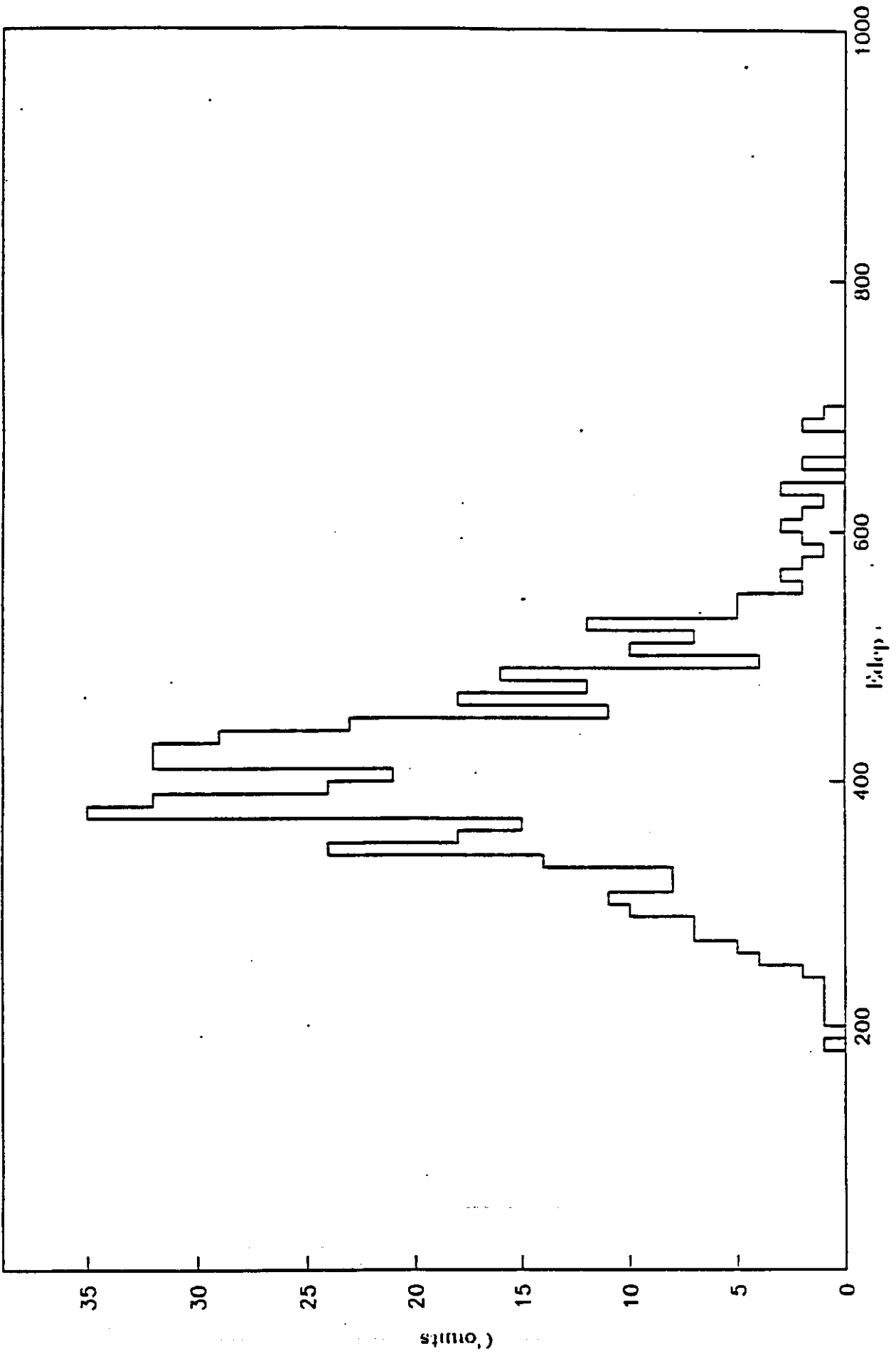
<u>Unit Cell (cm)</u>	<u>Particle Type</u>	<u>Spect</u>	<u>EGS</u>	<u>MORSE</u>	<u>TOTAL</u>	<u>RMS</u>	<u>(<math>\sigma/E</math>)</u>	<u><math>\sigma/\sqrt{E}</math></u>	<u><math>\frac{E}{\pi}</math></u>
FE-SCIN	$\pi^-$	75.4 ± 2.0	83.2 ± 2.0	9.4 ± 1.0	168.0 ± 5.0	30.4	18.1	57.2	1.24 ± 0.1
(1.76/0.25)	$\pi^-$	---	208.2 ± 3.0	---	208.2 ± 3.0	14.7	7.1	22.3	
PB-SCIN	$\pi^-$	199.7 ± 3.0	131.0 ± 2.0	81.5 ± 1.0	412.2 ± 6.0	51.6	12.5	39.6	1.04 ± 0.1
(0.56/0.25)	$\pi^-$	---	431.9 ± 5.0	---	431.9 ± 5.0	23.9	5.5	17.5	



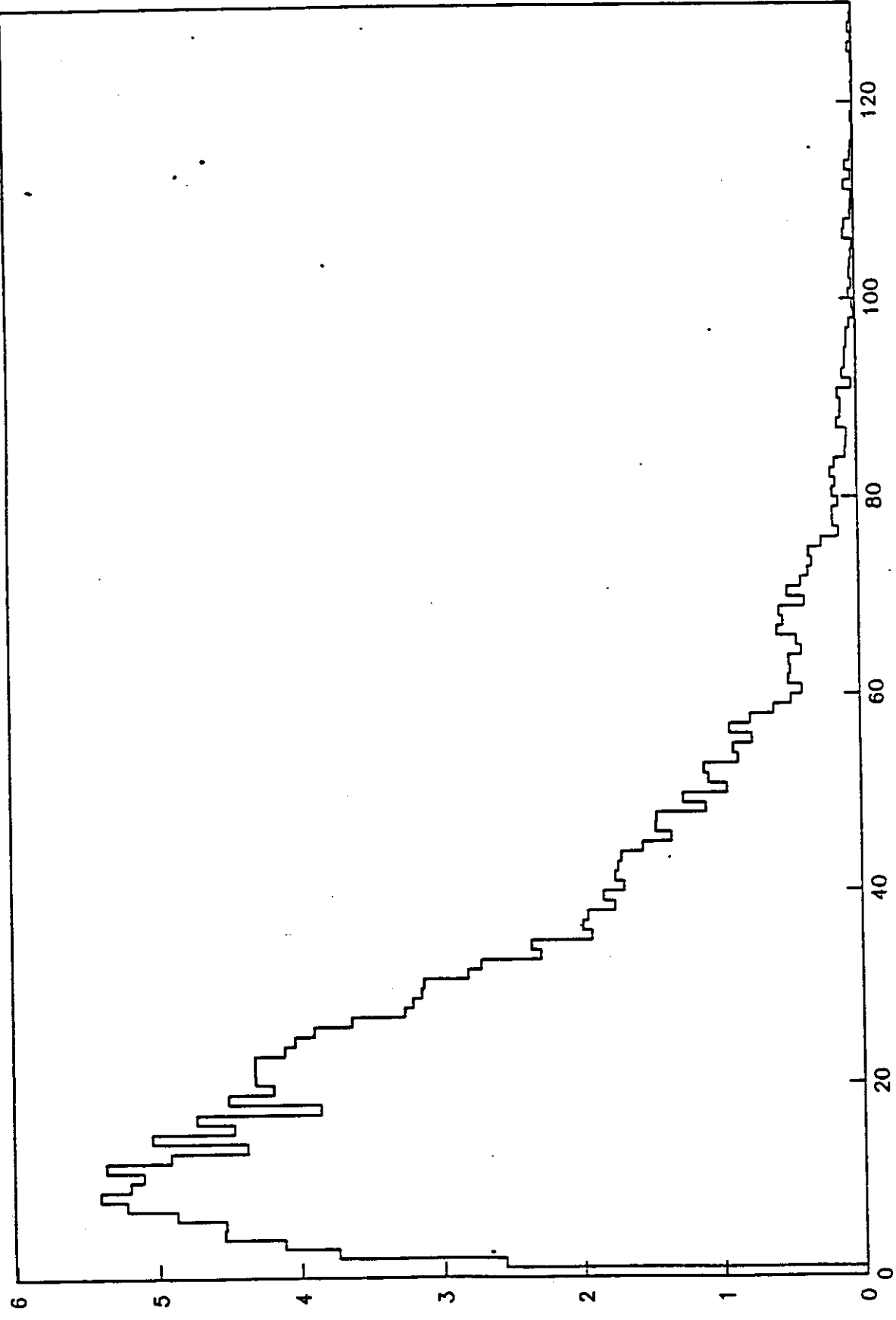
10 GEV ELECTRONS Pb-SCIN CONFIGURATION



10 GEV ELECTRONS PB-SCIN CONFIGURATION

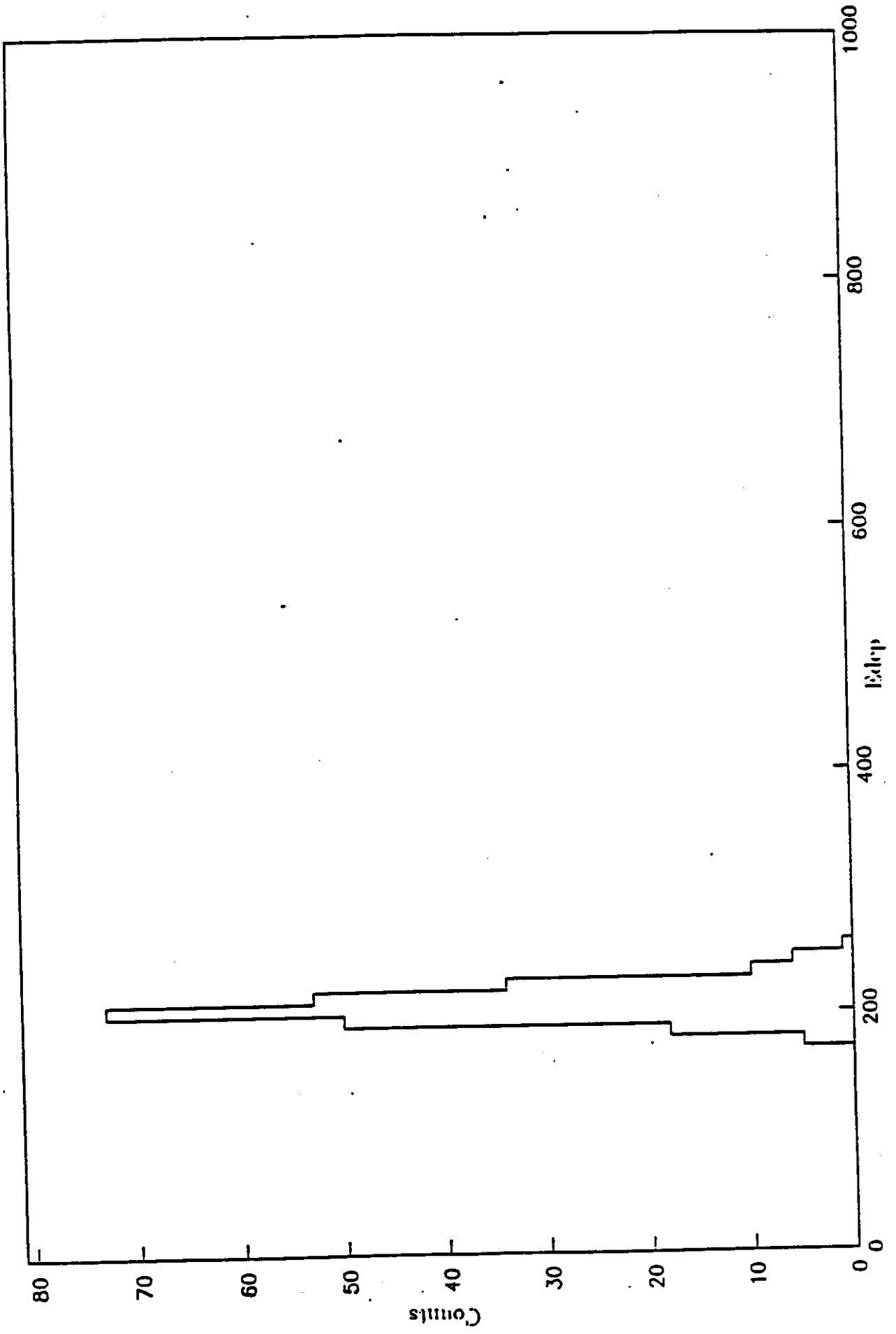


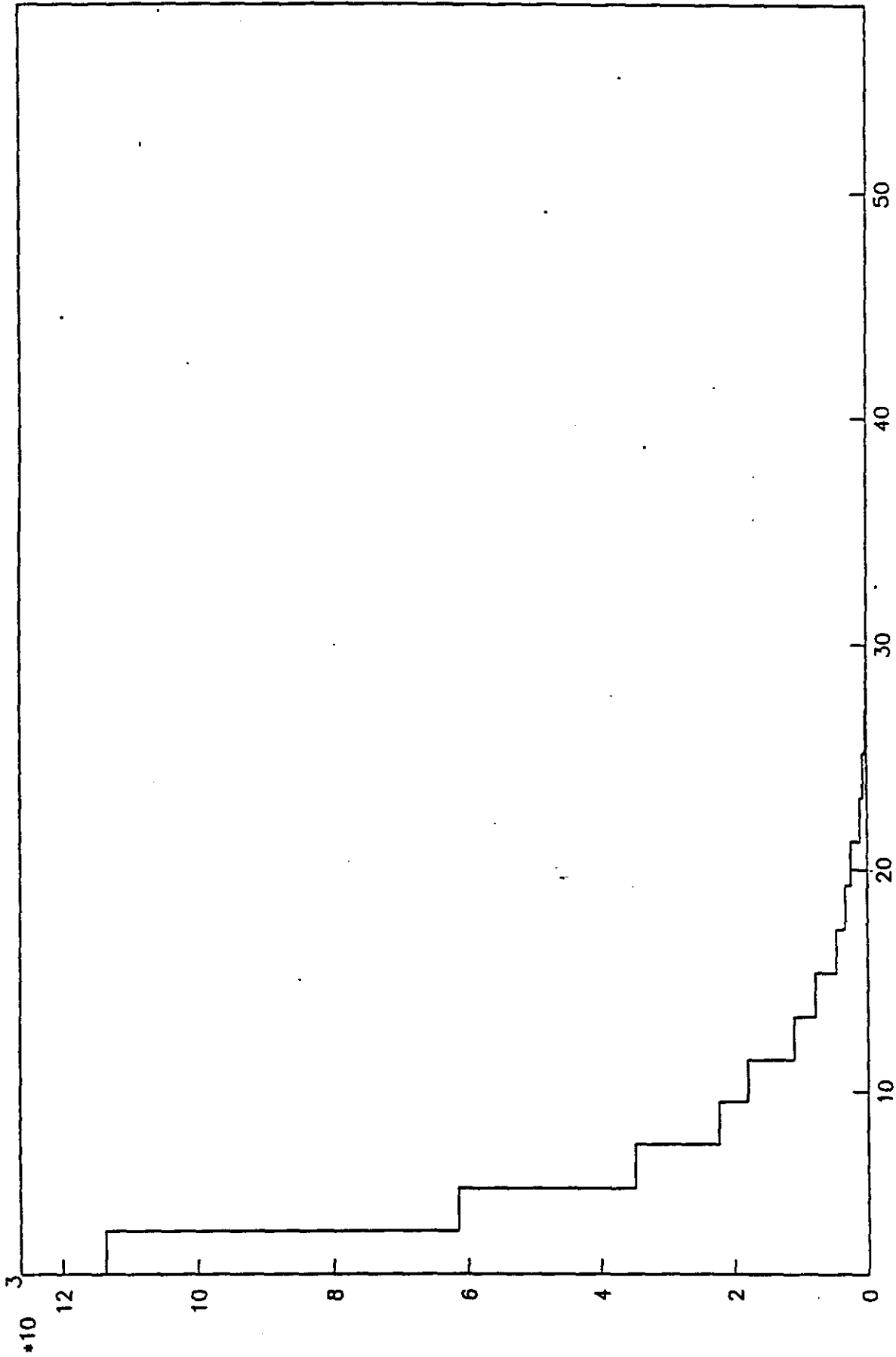
10 GEV PIONS Pb-SCIN CONFIGURATION



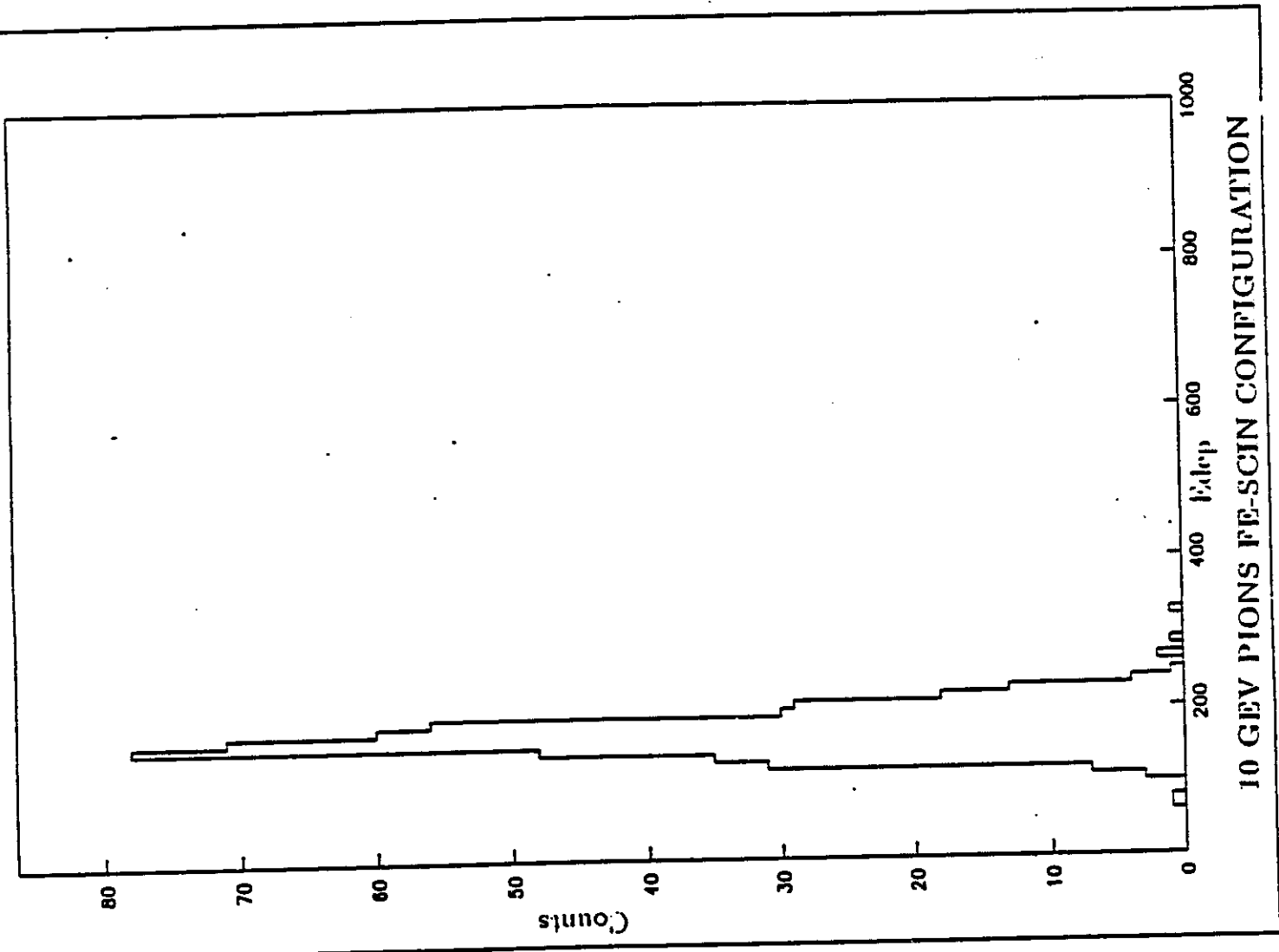
10 GEV PIONS PB-SCIN CONFIGURATION

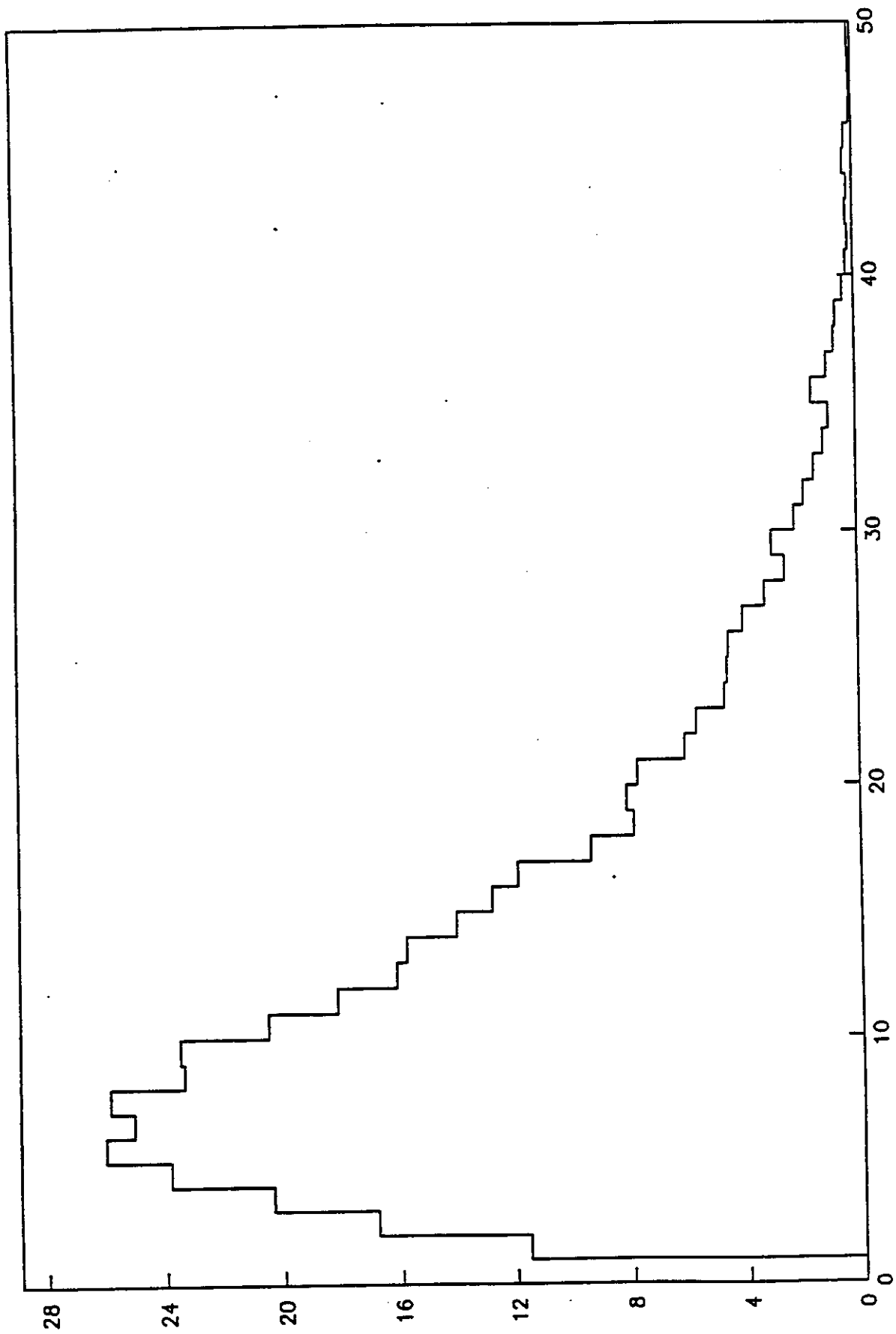
10 GEV ELECTRONS FE-SCIN CONFIGURATION





EDEP VS z (cm)  
10 GEV ELECTRONS FE-SCIN CONFIGURATION





LONGITUDINAL DIRECTION X0

10 GEV PIONS FE-SCIN CONFIGURATION

The submitted manuscript has been authored by a contractor of the U. S. Government under contract No. W-31-109-ENG-38. Accordingly, the U. S. Government retains a nonexclusive, royalty-free license to publish or reproduce the published form of this contribution, or allow others to do so, for U. S. Government purposes.

ANL-HEP-TR-90-77

SDC-90-00073

24 August 1990

A First Simulation Study  
of the Barrel-Endcap Transition Region  
in a Calorimeter of the Scintillator Tile Design\*

JAMES PROUDFOOT and HANS-JOCHEN TROST

*High Energy Physics Division - 362 -**Argonne National Laboratory**9700 S. Cass Ave., Argonne, IL 60439-4815, USA*

## ABSTRACT

We have made a first study of the calorimetric response to 10 GeV/c charged pions in the transition region between barrel and endcap for the scintillator-tile design pursued at Argonne National Laboratory using the simulation program ANLSIM. For (very nearly) projective tower orientations in the barrel, the crack appears deep within a narrow angular range, causing a loss of the response in that region up to 40 %. Pointing the towers onto the beam axis 35 cm or more away from the nominal interaction point leads to a shortened depth of the barrel-endcap crack as seen by particles incident from the interaction region, cutting the maximum loss down by almost one half. The worsening of the resolution follows the same trend. Introduction of a solenoidal coil in front of the calorimeter causes an overall degradation of the response by an amount nearly comparable to the effect of the crack. Electrons of the same incident momentum are more strongly affected by the coil than pions but see only a much narrower region of degradation by the crack.

---

\* Work supported by the U.S. Department of Energy, Division of High Energy Physics, Contract W-31-109-ENG-38

## 1. Introduction

Calorimeter designs for SSC detectors are often subject to a variety of mutually contradictory semi-hard requirements and boundary conditions. The underlying demands arise from the physics issues expected to be addressable by SSC experiments. These include hermeticity and homogeneity of the response over most of the solid angle and requirements on position and energy resolutions for electromagnetic and hadronic showers. In particular at the size scale to be considered at the SSC, the technical feasibility tends to create contradictions between those requirements. For instance, good spatial resolution is best achieved with a projective-tower readout geometry. This leads either to projective gaps ruining the hermeticity and local homogeneity of the response or to large cracks between large modules or to large amounts of nonsensitive materials in the region of the shower development.

In this note we present a simulation study of the barrel-endcap transition region for a calorimeter design as pursued at Argonne National Laboratory for a scintillator-tile sampling calorimeter.<sup>[1]</sup> In the following, we describe the tools and procedures used (section 2) and the results of the simulation runs and conclusions (section 3).

## 2. Tools and Procedures

The starting point for the present study is a design by N.Hill<sup>[1]</sup> shown in Fig.1. We have coded this geometry as shown in Fig.2 for use in the simulation program ANLSIM,<sup>[2]</sup> which is based on GEANT.<sup>[3]</sup> In the azimuthal direction, the setup is simplified for the simulation as being cylindrical everywhere. The tower geometry is coded and handled independently of the GEANT data structures. The simulation program is kept flexible with respect to the design by basing it on a number of parameters measuring various dimensions that can be set at runtime. Thus a design change can be accommodated without additional coding

and recompilation, within some limits. The relevant parameters are listed in Table 1. In this setup, the coil produces a homogeneous axial magnetic field of 2 T strength (dialed by input at run time) in the volume it encloses. There is no flux return modeled, so the calorimeter resides completely in a field free region. The essential features of this design for the present study are detailed in Appendix 1 which may serve as a guide to set the input variables for the program as well.

A set of options are investigated below making use of the selections offered in the program setup:

1. the standard design as given by N.Hill,<sup>[1]</sup> with 7 towers at the center oriented straight at a right angle to the beam axis, *i.e.* 3.5 on each side of  $z = 0$  m, four more towers maintaining the radial thickness of the barrel and pointing, like all further barrel towers, to  $z = 3.5 * towerwidth$ , and endcaps "fitting" into the conical end faces of the barrel with axially oriented towers of constant cross section; this is a nearly projective geometry in the barrel, avoiding the gaps between the barrel and the endcaps to point directly to the interaction point;
2. the strictly projective design, different from the standard simply by having no straight central towers;
3. further nonprojective designs like the standard one with the offset of 3.5 tower widths replaced by 1.5, 2, 2.5, 3, 5.5, 7.5 and 20 tower widths.

The variation the offset for projecting the towers determines the projectivity of the crack between the barrel and the endcap. In all cases, the endcap is moved in to just touch the aluminium support cones (1 inch thick) of the barrel. This leads to a minimal air gap. No material inside the volume enclosed by the calorimeter is simulated in the round through varying tower offsets; the magnetic field in that volume is taken present nevertheless. The calorimeter response is calibrated in the simulation for electromagnetic and hadronic energy depositions separately to recombine to an  $e/\pi$  ratio of close to 1.0 and to reproduce the absolute energy

scale, both to within about three percent.

For each setup, program runs are made sending negatively charged pions of momentum  $10 \text{ GeV}/c$  into the calorimeter at 14 values of pseudorapidity,  $\eta = 1.20, 1.30, 1.34 - 1.58$  in steps of 0.04, at 1.80 and intermediate points at 1.40 - 1.52, and randomly chosen azimuth  $\phi$ . The center of the gap between the barrel and the endcap is located around  $\eta = 1.44$ . The pion induced showers are simulated in ANLSIM using full analog simulation with relatively high cuts on the kinetic energies; they are set to  $100 \text{ MeV}$  to limit the execution times. This will misestimate the absolute resolution somewhat and also slightly reduce the shower size. It will nevertheless give a reasonable relative comparison of the design variants under consideration.

### 3. Results on Calorimeter Response

The total deposited energy before any clustering is performed is taken as the response of the calorimeter for the present purposes. The distributions of this energy normally contain about one thousand entries for each preset value of the pseudorapidity  $\eta$ . The results for three of the offsets investigated are collected in Table 2.

The calorimeter shows a flat response (Fig.3) of about  $10 \text{ GeV}$  with a deep dip of observable width in the gap between the barrel and the endcap developing as the tower orientation offset goes towards zero. (The error bars for the means in this figure show the r.m.s. value of the distribution and not the error of the mean, for the r.m.s. values, the error bars have no physical meaning at all.) At the "standard" design offset of  $35 \text{ cm}$ , the dip is a little more than 20 % for  $10 \text{ GeV}/c \pi^-$  incident, up from 40 % for the projective design, and has begun to level off in dependence on that offset (Fig.4). Adding more material in the gap will widen and deepen the dip in the response curve particularly for (nearly) projective designs. Choosing a point away from the deep-dip region as given by

the present study will then provide some safety margin against getting into the large uncertainties connected with the strong response variations:

We then include a simple model of the solenoidal coil in front of the calorimeter as shown in Fig.2 using the standard 35 cm tower projection offset and study the resulting response to pions (Fig.5). We find an overall degradation of more than 10 % within the solid angle coverage of the coil with only half of that effect in the crack-related dip. Clearly, the coil as modeled provides a scattering center in front of the crack that spreads the energy deposition beyond the coil into the sensitive regions of the calorimeter. The range in pseudorapidity affected by the coil end is about  $\eta = 1.42 - 1.52$  and the resolution is degraded by less than 30 %. This is certainly a somewhat too optimistic picture of the reality since there may be more material in the coil end itself (we use a massive aluminium ring of thickness 15 cm along the beam axis and 30 cm radially) and will be more material for support of tracking systems and supplies for everything inside the volume enclosed by the calorimeter. For comparison, the simulation efforts for the SDC Expression of Interest<sup>[4]</sup> assume the range of degradation to be  $\eta = 1.25 - 1.5$  and the increase of the resolution up to 70 %.

An additional check on the performance for the standard geometrical choice is to look at the response and acceptance for electrons. We performed runs for the standard design without and with coil in place for electrons of 10 GeV/c momentum. For the set and density of points in pseudorapidity used, the crack produces a very deep but also narrow ( $\Delta\eta \approx 0.01$  wide) dip in the response. The coil takes much more energy away from the electrons than from pions as has to be expected (Fig.6) and also worsens the response in the dip significantly. This means the design under consideration essentially will have a narrow ring almost blind to electrons of moderate energies. This is probably acceptable unless the gap has to be widened for hardware support installations a lot.

To conclude, we have obtained support from full simulations of pion showers for a preference of using a quite moderately nonprojective tower geometry in the

absorber-scintillator tile calorimeter as considered for SDC. The tower orientation determines the orientation of the gaps in the calorimeter coverage, and it is these gaps that have to be well covered by active detectors in a view from the interaction point. The impact of having a solenoidal coil in front of the barrel calorimeter the ends of which reach into the barrel-endcap region is in size comparable to the effect of the crack itself. In the final detector, the crack will contain more material than only the support cones for the barrel calorimeter. For that total amount of passive material, the 1 *inch* thickness of the support cones is a very crude and possibly thin approximation. In continuing this study, we will look at the impact on particle and jet reconstruction in some detail, and we will also attempt to improve the geometry to reflect more realistically the dead material needed by the detectors and the simulation technique to study higher particle energies.

## APPENDIX 1

The following is a detailed description of the structure of the geometry setup used in ANLSIM:

1. The central towers in the barrel are oriented strictly at a right angle with respect to the beam axis, thus they are not projective in the  $(r, z)$  plane (where  $r$  denotes the radius in the plane transverse to the beam axis). The number of these towers, counted from  $z = 0$  to one side only, is given in the variable BARTOF. In the range of these towers the total transverse thickness of the barrel calorimeter is set by the variable BARDRC. The side length of the central towers at their front face is taken to be BARTOW.
2. At the front faces, a conical shell of aluminium of thickness BARCON is attached to support the barrel.
3. By projecting the outside boundary of the central towers onto the beam axis, a secondary origin is defined. From this origin outward, i.e. away from the main coordinate origin, a pseudorapidity variable is used to define the polar boundaries of the remaining barrel towers. A constant stepping in pseudorapidity produces a constant *projected* size of the towers at the inner surface of the barrel (see appendix 2). The same side length BARTOW is imposed here for the projected size that is used for the central towers also. Thus, a strictly projective tower geometry in the barrel can be produced by having zero central towers as defined above; this is in fact allowed by the simulation program. In turn, an extremely nonprojective geometry can be defined by making the central towers extend over most of the barrel range. This range or half length at the inside surface is defined as the half length of the coil COILZE plus an extension BAREXT over this point, truncated to the largest number of complete towers that can be contained in this bound.
4. Across the first BARTOF towers in the - relative to the secondary origin - projective region, the central transverse thickness of the calorimeter is

maintained. Beyond those, the outer transverse radius decreases linearly with the axial coordinate  $z$  to produce an outer side length BARDRE of the "last" ring of barrel towers. (That length is measured on a ray from the secondary origin along the side face of the towers.)

5. The endcaps are constructed as thick cylinders (length/depth ENDDZC, radial extent ENDDRT starting at an inner radius ENDRIN), with a few (ENDDRI) rings within the radial extent reduced in depth on the inside and a larger number (ENDNST) of rings added on the outside to form an approximation to a conical shape. The inside rings follow a cone with its apex at the primary origin. The outer rings are aligned to have their edges at a constant distance from the outermost ring of barrel towers, i.e. they follow a cone parallel to the cone with an apex slightly further out than the secondary origin and an angle given by the end face of the barrel. The placement of the whole endcaps along the beam axis is governed by the half length COILZH of the coil and the gap width ENDGAP between the coil and the front face of the endcap. The towers are oriented axially, i.e. not projective; this feature is fixed.
6. The outer rings of the endcaps are divided into a short and a long remnant piece each such that the short rings just overlap by a given amount ENDRGO. The idea is to allow to form pseudotowers on the endcap side of the gap between the barrel and the endcap that approximately continue the tower structure of the barrel by one more layer. This could be useful for pattern recognition across that gap. In the present study, this feature has not been used and the short pieces are effectively joint with the longer remnants into one piece.
7. The azimuthal subdivision throughout all of the calorimeter parts is chosen to give a width at the inner face of the calorimeter as close to the desired tower side length (BARTOW and ENDTOW resp.) as possible under the restriction of having an integral number of towers around the azimuthal

circumference. (This will give an inaccurate model of the performance of pattern recognition in the endcap region; for the current purpose, this does not matter.)

8. The whole calorimeter is subdivided into one longitudinal electromagnetic section of transverse/axial thickness BARDEM and ENDDM resp., and one hadronic section.
9. Each tower (electromagnetic and hadronic separately) is assigned artificially a coordinate in the pseudorapidity-azimuth plane  $(\eta, \phi)$  as follows:
  - (a) The  $\phi$  coordinate is taken at the azimuthal center of the tower in all cases.
  - (b) The  $\eta$  coordinate for the electromagnetic towers is taken at the halfway point into the tower on their center lines.
  - (c) The  $\eta$  coordinate for the hadronic towers in the barrel and in the main body of the endcap is taken 1.5 times the depth of the electromagnetic section (not the length of the tower in front), *i.e.* BARDEM and ENDDM resp., into the hadronic section at right angles, *not* measured along the center lines of the towers.
  - (d) In the rings of the endcaps, the assigned *eta* coordinates are picked on cones connecting to the plane used in the main body, with a cone angle taken wide enough to conserve the spatial radial order of rings of towers in the pseudorapidity order.
10. The detector geometry can be extended (via input flags at run time) to include a beam pipe, a coil, a model of an all-scintillating-fiber tracker, and a muon system. The coil parameters are used in the setup of the calorimeter as is evident above; they are available and modifiable even if no actual placement of the coil into the geometry setup to be known by ANLSIM/GEANT is requested.

The routines needed to define and use the setup are kept in a separate file, replacing the default ones of ANLSIM at linking time.

## APPENDIX 2

The equivalence of constant tower size in the pseudorapidity coordinate  $\eta$  and in projected size (side length  $2 \cdot \Delta w$ ) at the inside of a cylinder of inner radius  $R_0$  can be seen as follows:

Let the ray from the interaction point into the center of a tower have the polar angle  $\Theta$  with respect to the beam axis. Then the half width  $\Delta w$  of the tower is related to a deviation of the polar angle

$$\Delta w = \frac{R_0}{\sin(\Theta)} \tan(\Delta\Theta) .$$

In order to study the angular dependence of the "cumulated half widths" function  $w$ , let us use in the limit of small angular deviations the approximation of the tangent function by its argument,

$$\tan(\Delta\Theta) \rightarrow \Delta\Theta .$$

This substitution leaves the limit  $\Delta\Theta \rightarrow 0$  of  $\Delta w$  invariant, being

$$\frac{dw}{d\Theta} = \frac{R_0}{\sin(\Theta)} ,$$

as the difference  $\tan(\Delta\Theta) - \Delta\Theta$  is continuously differentiable in a whole neighborhood of zero and it and its first derivative vanish at zero (the former quadratically as its Taylor series exists and converges in that region). By integration from  $\Theta = \pi/2$  to any polar angle we find<sup>[9]</sup> for the function  $w$  the representation

$$w(\Theta) = R_0 \ln\left(\tan\left(\frac{\Theta}{2}\right)\right) = -R_0 \eta .$$

Thus, the request arising from the physics of jets to define towers with constant width on the (pseudo-) rapidity scale and that one arising from pattern recognition to define towers of constant width across the lateral extension of showers

actually coincide in a cylindrical calorimeter aligned on the beam axis. This coincidence is lost in the endcaps where  $\Delta w$  has a different dependence on  $\Theta$ .

## REFERENCES

- 1) N.Hill, Observations and conclusions drawn from conceptual design exercises on barrel calorimeter for SDC, internal note, Argonne National Laboratory, May 30, 1990 (unpublished)
- 2) R.E.Blair, L.E.Price and H.-J.Trost, program ANLSIM, Argonne National Laboratory, Argonne, Illinois, USA 1989, version 1.04, 1990, unpublished;  
H.-J.Trost, talk given at: Workshop on the Future Development of GEANT, SSC Laboratory, Dallas, Texas, Jan.10-13, 1990, unpublished;  
R.E.Blair, in: Workshop on Physics and Detector Simulation for SSC Experiments, SSC Laboratory, Dallas, Texas, Jan.9-19, 1990, vol.1, p.69;  
H.-J.Trost, *ibid.*, vol.2, p.265
- 3) R.Brun *et al.*, GEANT 3, CERN DD/EE/84-1, version 3.13, CERN, Geneva, Switzerland 1990
- 4) Solenoid Detector Collaboration, Expression of Interest to Construct and Operate a Detector at the SSC, May 24, 1990
- 5) I.N.Bronshtein and K.A.Semendyayev, Handbook of Mathematics, 3rd English edition, Van Nostrand Reinhold Company, New York, New York, USA 1985, section 1.1.3

## TABLE CAPTIONS

1. Design parameters used in the geometry setup for ANLSIM (lengths in *cm*; defaults in parentheses)
2. Pseudorapidity, polar angle, momentum components, mean response and r.m.s. of the response for a) the standard design, b) the projective design, c) the highly nonprojective design with 2 *m* offset

## FIGURE CAPTIONS

1. Side view of the calorimeter design addressed in this study
2. Side view of the mechanical calorimeter geometry as seen by the ANLSIM program - standard design with optional coil
3. Mean response and resolution for 10 *GeV/c*  $\pi^-$  of the calorimeter of ref.1 for different offsets of the tower orientation; the errors on the mean shown are the resolutions, and the error bars shown for the resolution have no physical meaning
4. Minimum response to 10 *GeV/c*  $\pi^-$  in dependence on the tower projection offset; the additional star for 35 *cm* offset shows the effect of the solenoidal coil.
5. Mean response and resolution for 10 *GeV/c*  $\pi^-$  of the calorimeter of ref.1 without and with coil in place
6. Mean response and resolution for 10 *GeV/c*  $e^-$  of the calorimeter of ref.1 without and with coil in place

Table 1

PIPEIN	inner radius of Beryllium beam pipe (4.9)
PIPEDR	thickness of beryllium beam pipe (0.1)
COILIN	inner radius of inner coil shell (185.0)
COILMI	inner radius of central coil shell (198.5)
COILUT	outer (!) radius of outer coil shell (215.0)
COILZH	axial half length of coil (450.0)
COILEN	axial length of massive coil end pieces (10.0)
COILD1	radial thickness of inner coil shell (3.0)
COILD2	radial thickness of central coil shell (3.0)
COILD3	radial thickness of outer coil shell (3.0)
BAREXT	axial extension on each side of the front face of the barrel calorimeter (5.0)
BARGAP	radial space between outside radius of coil and the barrel calorimeter (10.0)
BARDRC	total radial thickness of barrel at z=0 (234.9)
BARTOF	number of towers from center out that have constant width in z (3.5)
BARTOH	number of additional towers beyond the constant width ones for which the radial thickness of the barrel remains constant (4.0)
BARDRE	total depth of barrel along side to end cap (243.8)
BARDEM	thickness of electromagnetic barrel section (19.3=7.592*2.54)
BARTOW	projected azimuthal front width of towers (10.0)
BARCON	thickness of aluminium support cone at end faces (2.5)
ENDGAP	space between coil end and front face of end cap (25.0)
ENDRIN	inner radius at front face of end cap (50.0)
ENDDRT	radial thickness of end cap at front face (180.0)
ENDDRI	radial number of inner towers shorter than full axial thickness of end cap (3.0)
ENDDZI	length of innermost hadronic endcap towers (12.8)
ENDDZC	axial thickness of end cap (278.2=375*0.292*2.54)
ENDDEM	thickness of electromagnetic end cap section (19.3=7.592*2.54)
ENDRGO	axial overlap of rings (2.3=3*0.292*2.54)
ENDTOW	side length of end cap tower (10.0)
ENDNST	number of steps for outside rings of end caps (11)

Table 2a

eta	theta [degrees]	pz [GeV/c]	pT of events	number of events	<E(obs.)> [GeV]	r.m.s. [GeV]
0.00	90.00	0.000	10.000	1000	10.16	1.25
1.20	33.50	8.337	5.523	1000	10.17	1.20
1.30	30.50	8.617	5.074	1000	10.10	1.30
1.34	29.35	8.717	4.901	1000	10.14	1.21
1.38	28.24	8.810	4.732	1000	10.04	1.26
1.40	27.71	8.854	4.649	1000	10.12	1.32
1.41	27.44	8.875	4.608	1000	10.05	1.28
1.42	27.18	8.896	4.567	1000	10.07	1.24
1.43	26.92	8.917	4.527	1000	9.91	1.39
1.44	26.66	8.937	4.487	1000	9.41	1.39
1.45	26.40	8.957	4.447	1000	7.72	1.97
1.46	26.15	8.977	4.407	1000	9.44	1.57
1.47	25.90	8.996	4.368	1000	9.79	1.31
1.48	25.65	9.015	4.328	1000	9.92	1.30
1.49	25.40	9.033	4.290	1000	10.00	1.32
1.50	25.16	9.051	4.251	1000	10.04	1.26
1.52	24.67	9.087	4.175	1000	10.14	1.26
1.54	24.20	9.121	4.099	1000	10.13	1.25
1.58	23.28	9.186	3.952	1000	10.14	1.32
1.80	18.77	9.468	3.218	1000	10.18	1.26

Table 2b

eta	theta [degrees]	pz [GeV/c]	pT of events	number of events	<E(obs.)> [GeV]	r.m.s. [GeV]
0.00	90.00	0.000	10.000	1000	10.16	1.16
1.20	33.50	8.337	5.523	1000	10.09	1.40
1.30	30.50	8.617	5.074	1000	10.09	1.41
1.34	29.35	8.717	4.901	1000	10.13	1.35
1.38	28.24	8.810	4.732	1000	10.15	1.39
1.40	27.71	8.854	4.649	1000	9.94	1.32
1.41	27.44	8.875	4.608	1000	9.85	1.37
1.42	27.18	8.896	4.567	1000	6.95	2.08
1.43	26.92	8.917	4.527	1000	6.06	3.27
1.44	26.66	8.937	4.487	1000	9.26	1.60
1.45	26.40	8.957	4.447	1000	9.73	1.51
1.46	26.15	8.977	4.407	1000	10.04	1.31
1.47	25.90	8.996	4.368	1000	10.02	1.29
1.48	25.65	9.015	4.328	1000	10.00	1.33
1.49	25.40	9.033	4.290	1000	10.13	1.34
1.50	25.16	9.051	4.251	1000	10.14	1.39
1.52	24.67	9.087	4.175	1000	10.15	1.22
1.54	24.20	9.121	4.099	1000	10.20	1.28
1.58	23.28	9.186	3.952	1000	10.11	1.29
1.80	18.77	9.468	3.218	1000	10.15	1.31

Table 2c

eta	theta	pz	pT	number	<E(obs.)>	r.m.s.
	[degrees]	[GeV/c]	of events		[GeV]	[GeV]
0.00	90.00	0.000	10.000	1000	10.21	1.26
1.20	33.50	8.337	5.523	1000	10.15	1.31
1.30	30.50	8.617	5.074	1000	10.22	1.32
1.34	29.35	8.717	4.901	1000	10.10	1.28
1.38	28.24	8.810	4.732	1000	9.91	1.37
1.40	27.71	8.854	4.649	1000	9.78	1.33
1.41	27.44	8.875	4.608	1000	9.70	1.42
1.42	27.18	8.896	4.567	1000	9.55	1.57
1.43	26.92	8.917	4.527	1000	9.72	1.43
1.44	26.66	8.937	4.487	1000	9.96	1.39
1.45	26.40	8.957	4.447	1000	10.06	1.29
1.46	26.15	8.977	4.407	1000	9.99	1.34
1.47	25.90	8.996	4.368	1000	10.08	1.36
1.48	25.65	9.015	4.328	1000	10.12	1.21
1.49	25.40	9.033	4.290	1000	10.11	1.25
1.50	25.16	9.051	4.251	1000	10.09	1.29
1.52	24.67	9.087	4.175	1000	10.18	1.26
1.54	24.20	9.121	4.099	1000	10.18	1.21
1.58	23.28	9.186	3.952	1000	10.06	1.25
1.80	18.77	9.468	3.218	1000	10.20	1.22

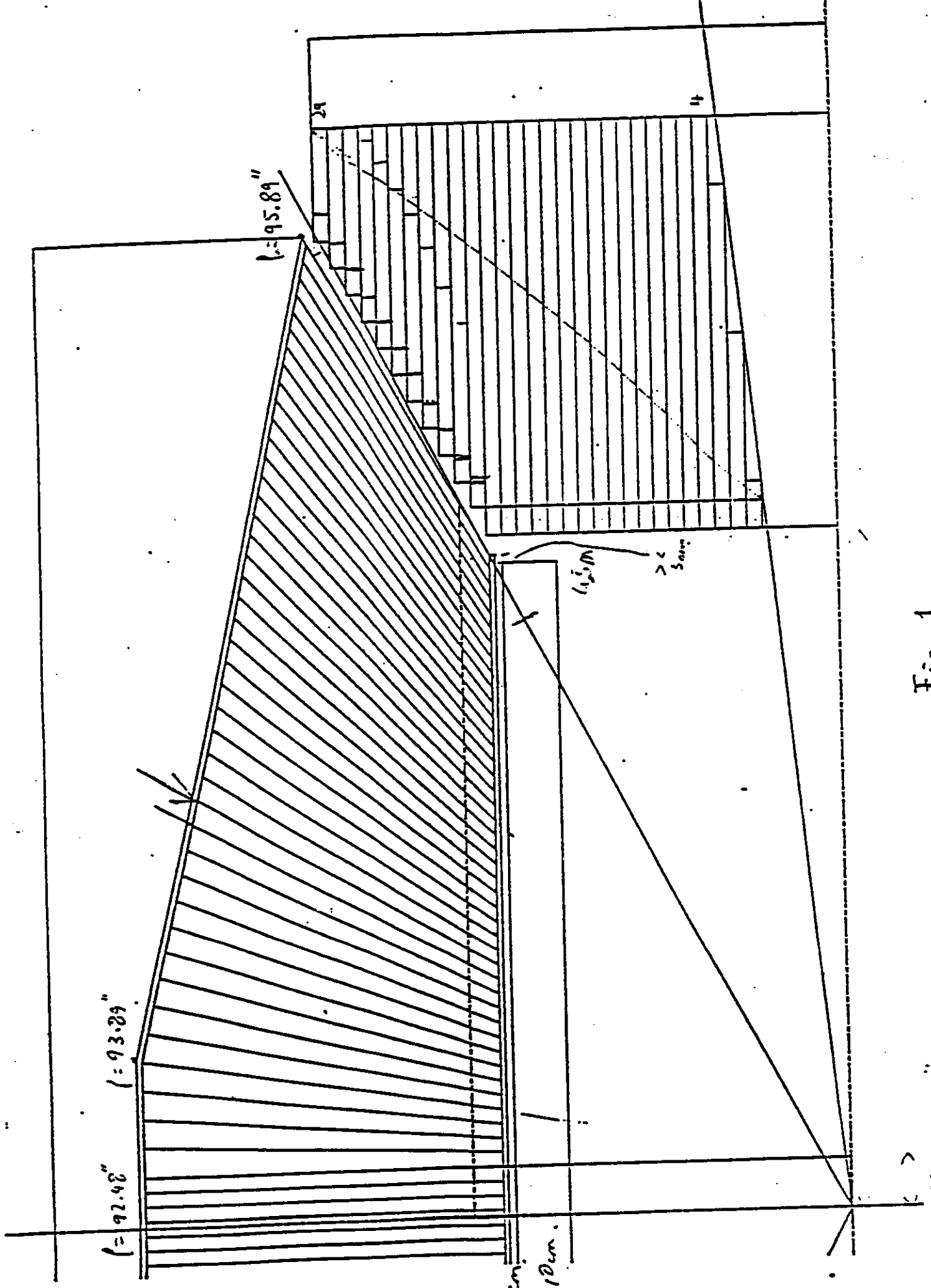


Fig. 1

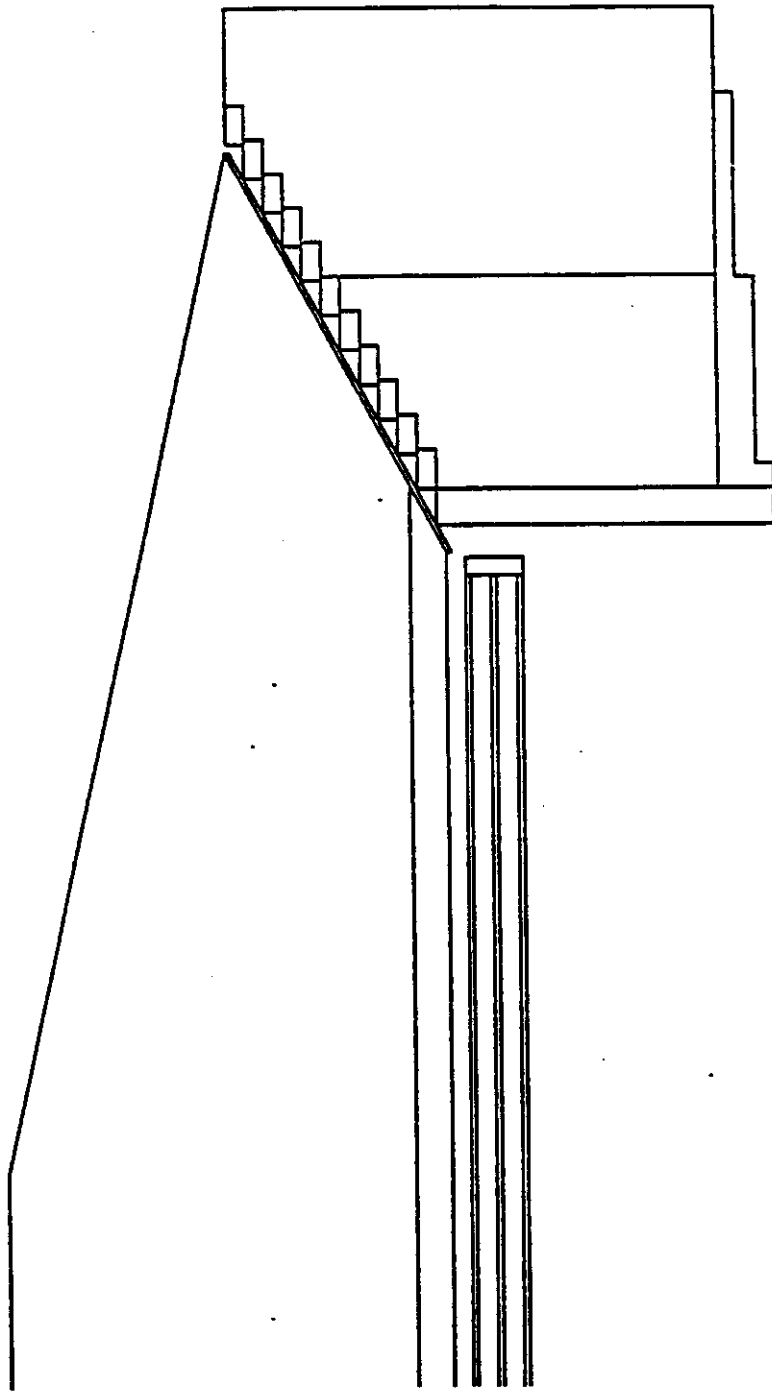
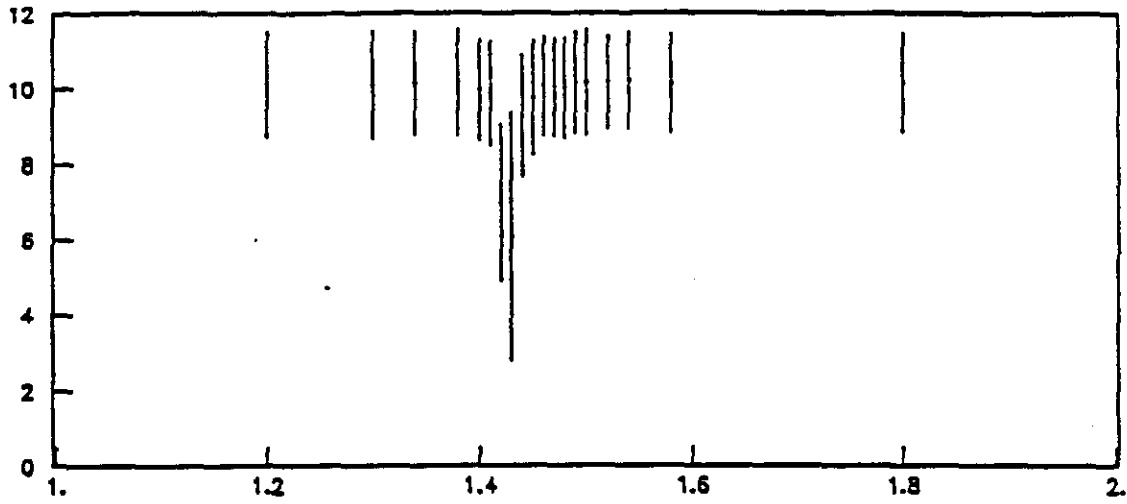
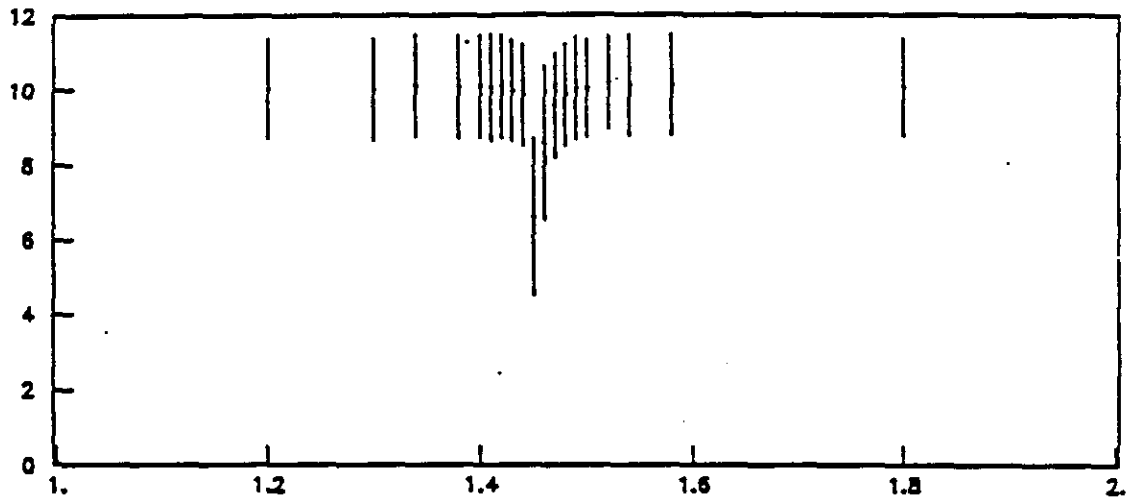


Fig. 2

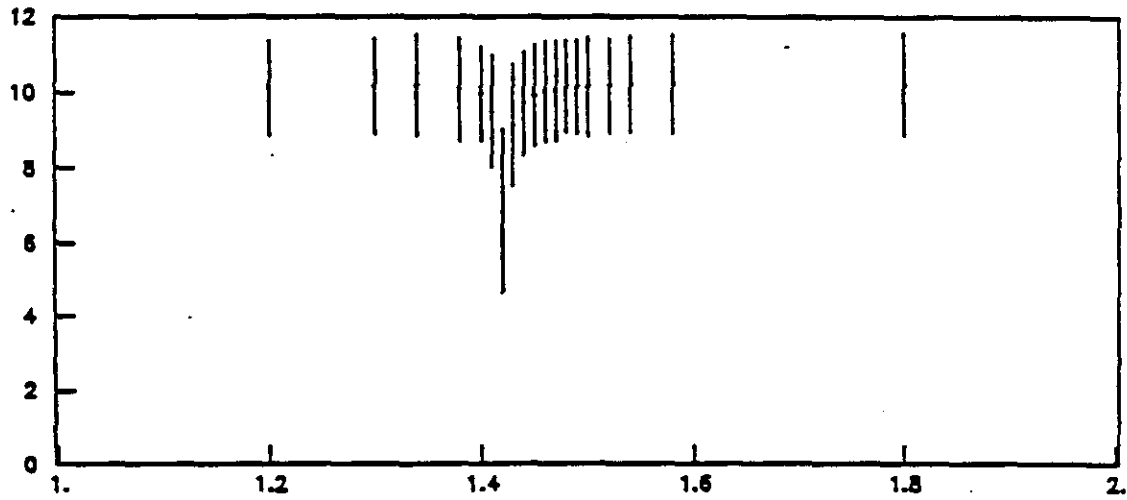
Calorimeter response over  $\eta$



$\langle E_{cal} \rangle$  - Strictly projective barrel



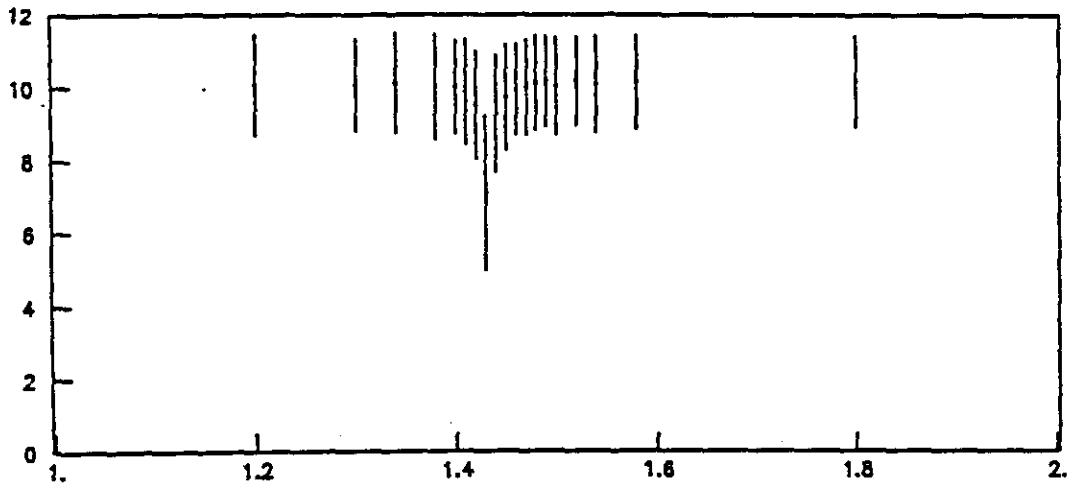
$\langle E_{cal} \rangle$  - Projection offset 15 cm no coil



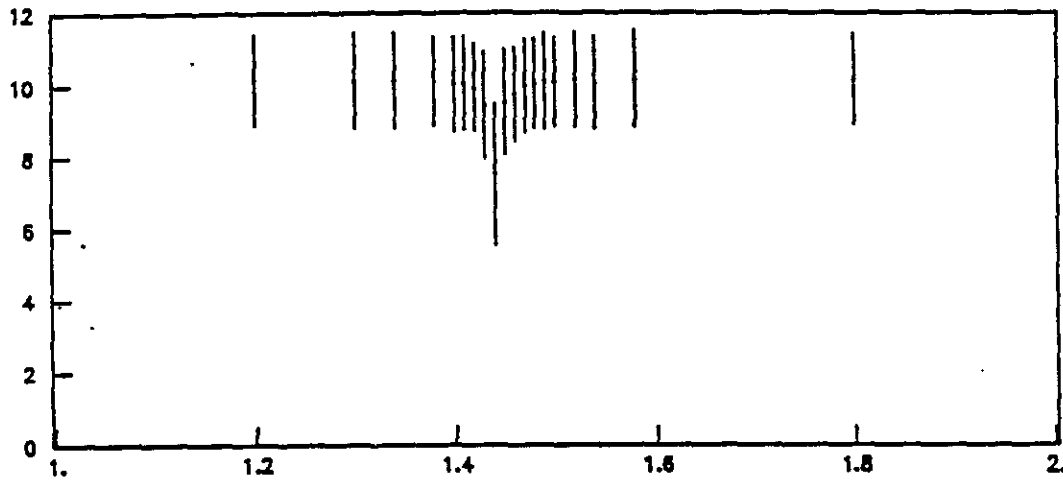
$\langle E_{cal} \rangle$  - Projection offset 20 cm no coil

Fig. 3 (1 of 6)

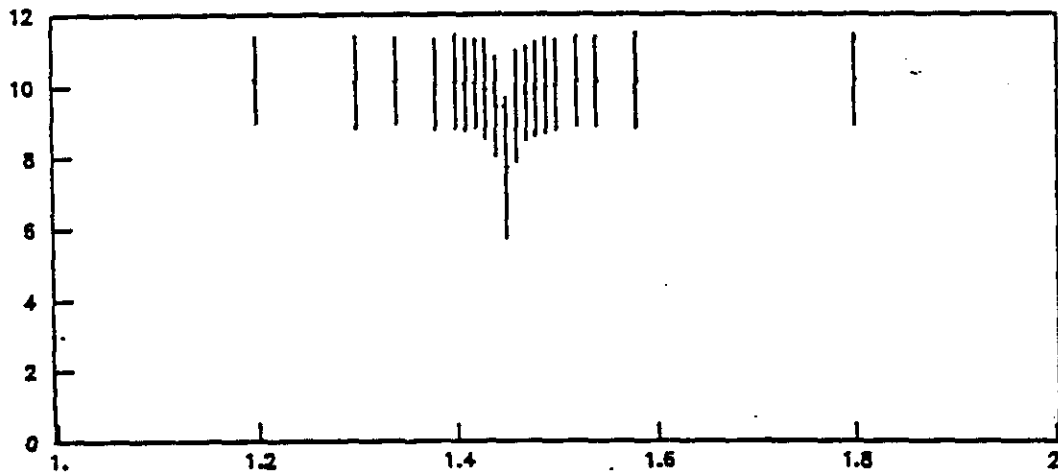
Calorimeter response over  $\eta$



$\langle E_{cal} \rangle$  - Projection offset 25 cm. no coil



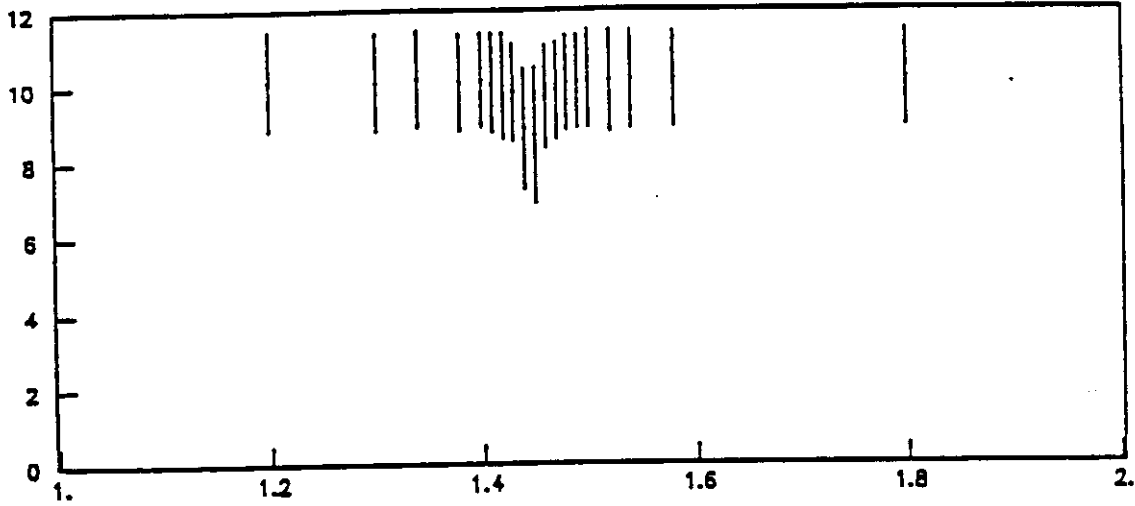
$\langle E_{cal} \rangle$  - Projection offset 30 cm. no coil



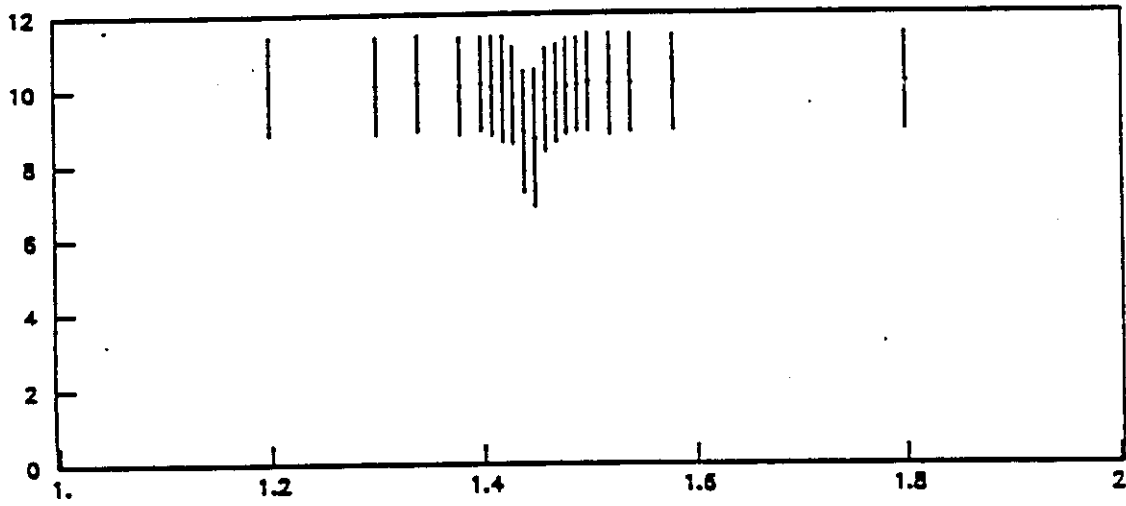
$\langle E_{cal} \rangle$  - Projection offset 35 cm. no coil

Fig. 3 (2 of 6)

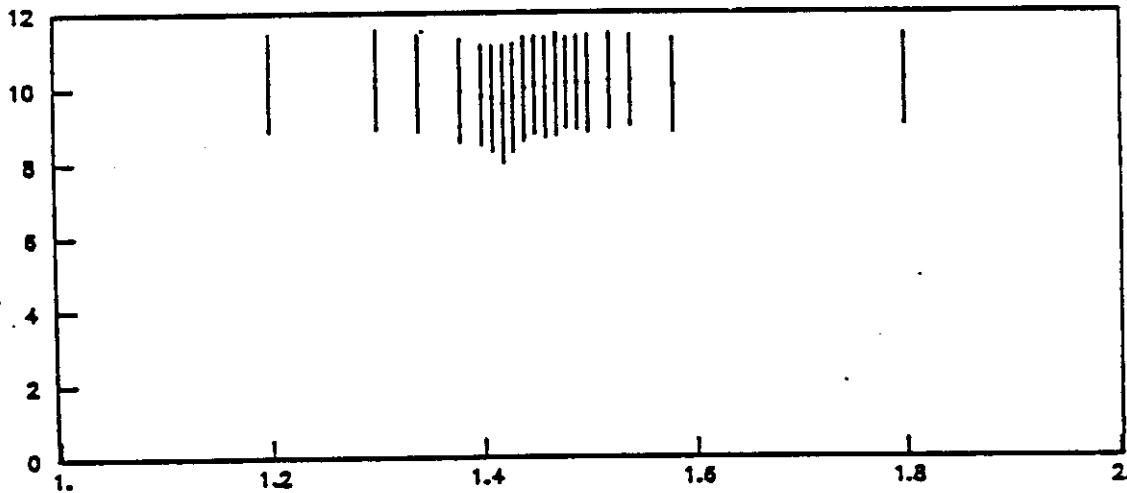
Calorimeter response over  $\eta$



$\langle E_{cal} \rangle$  - Projection offset 55 cm no coil



$\langle E_{cal} \rangle$  - Projection offset 75 cm no coil



$\langle E_{cal} \rangle$  - Projection offset 200 cm no coil

Fig. 3 (3 of 6)

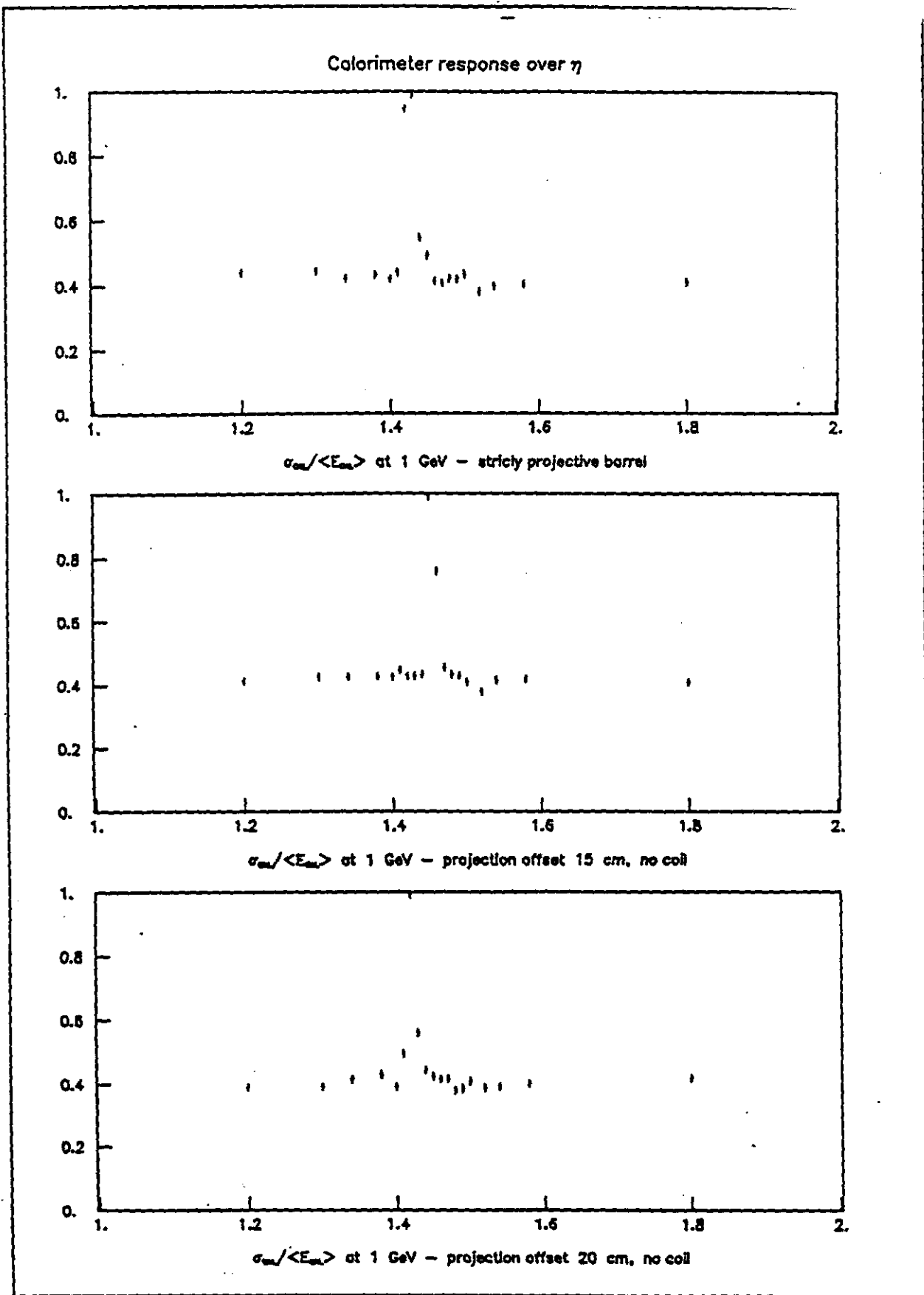
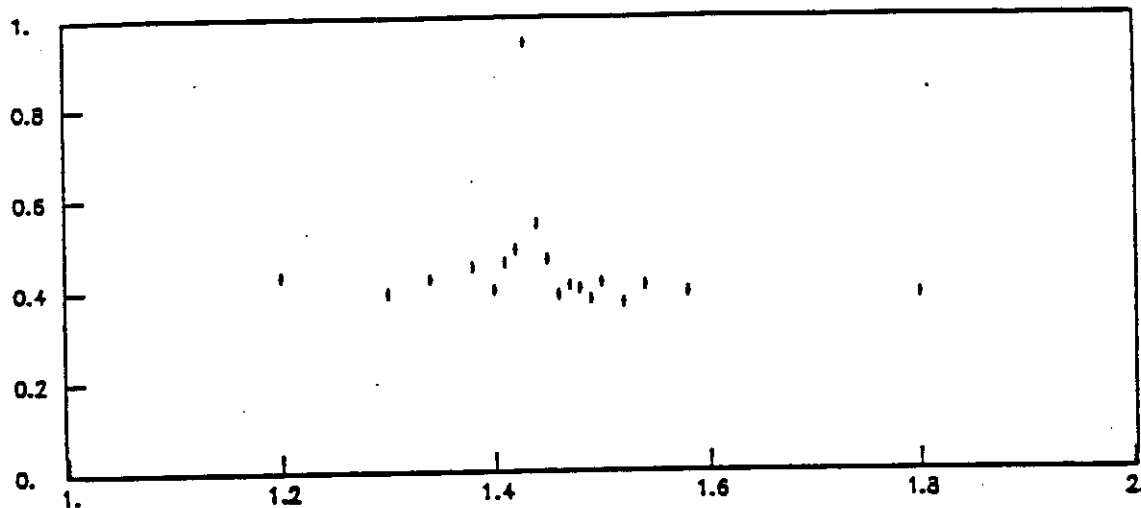
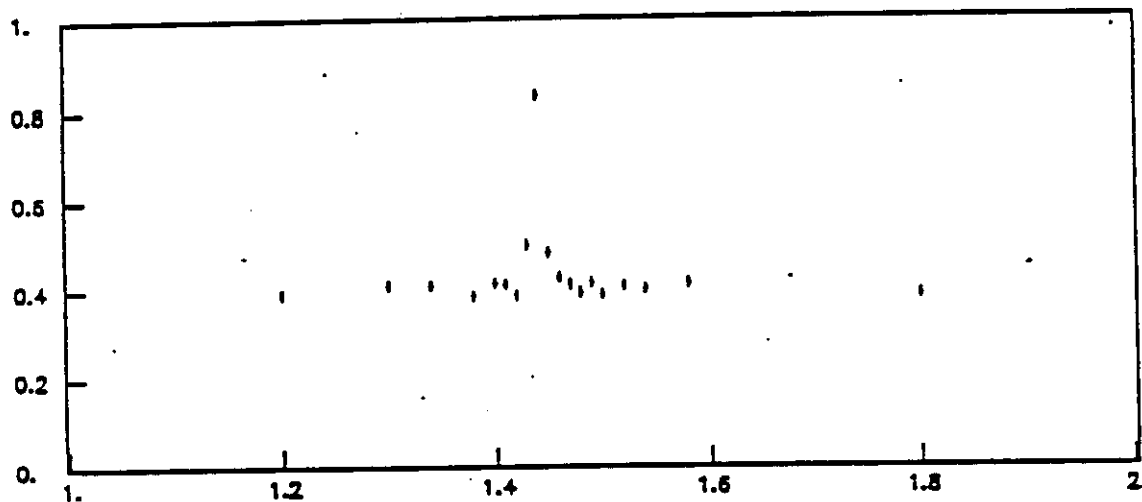


Fig. 3 (4 of 6)

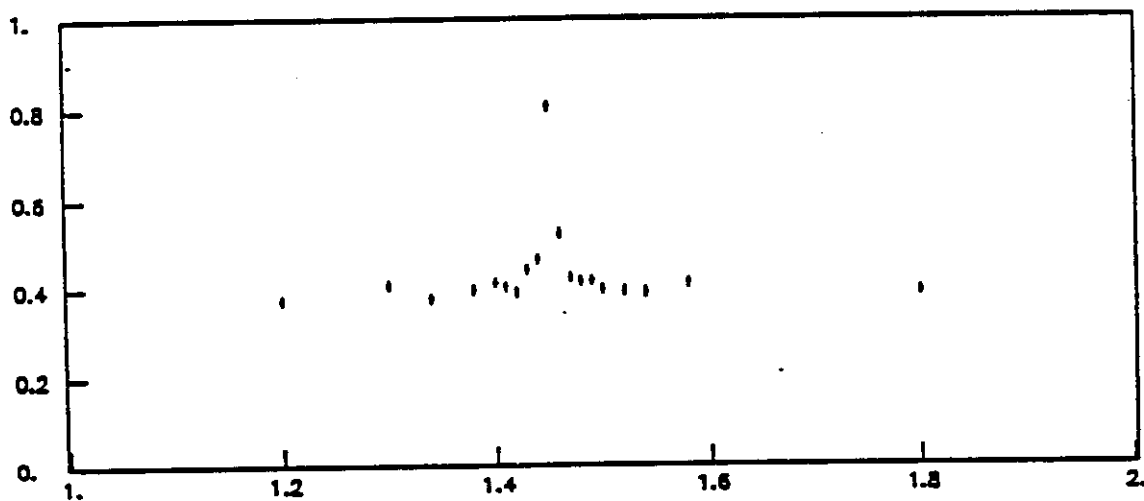
Calorimeter response over  $\eta$



$\sigma_{cal}/\langle E_{cal} \rangle$  at 1 GeV - projection offset 25 cm, no coil



$\sigma_{cal}/\langle E_{cal} \rangle$  at 1 GeV - projection offset 30 cm, no coil



$\sigma_{cal}/\langle E_{cal} \rangle$  at 1 GeV - projection offset 35 cm, no coil

Fig. 3 (5 of 6)

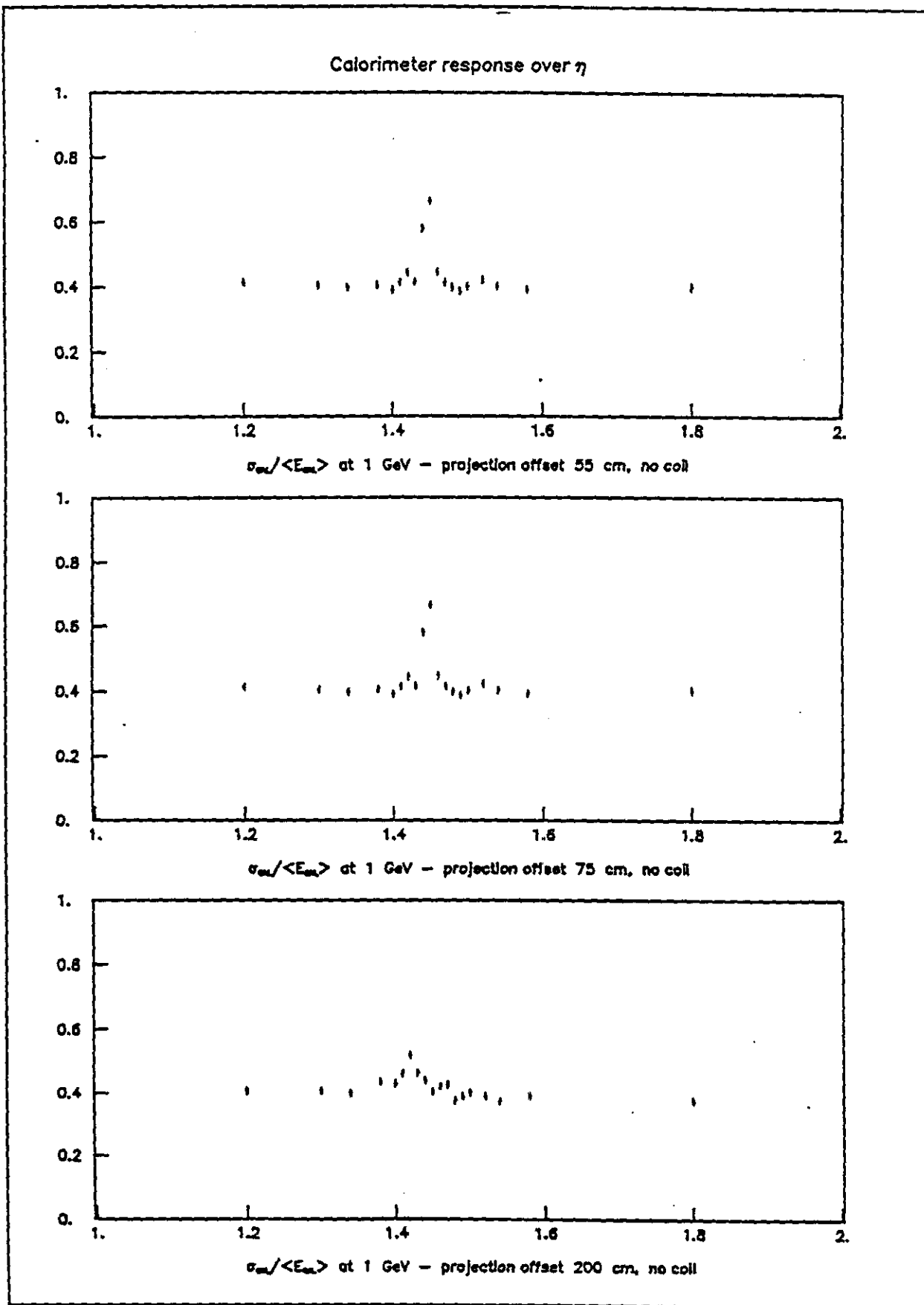


Fig.3 (6 of 6)

Minimal response in transition region

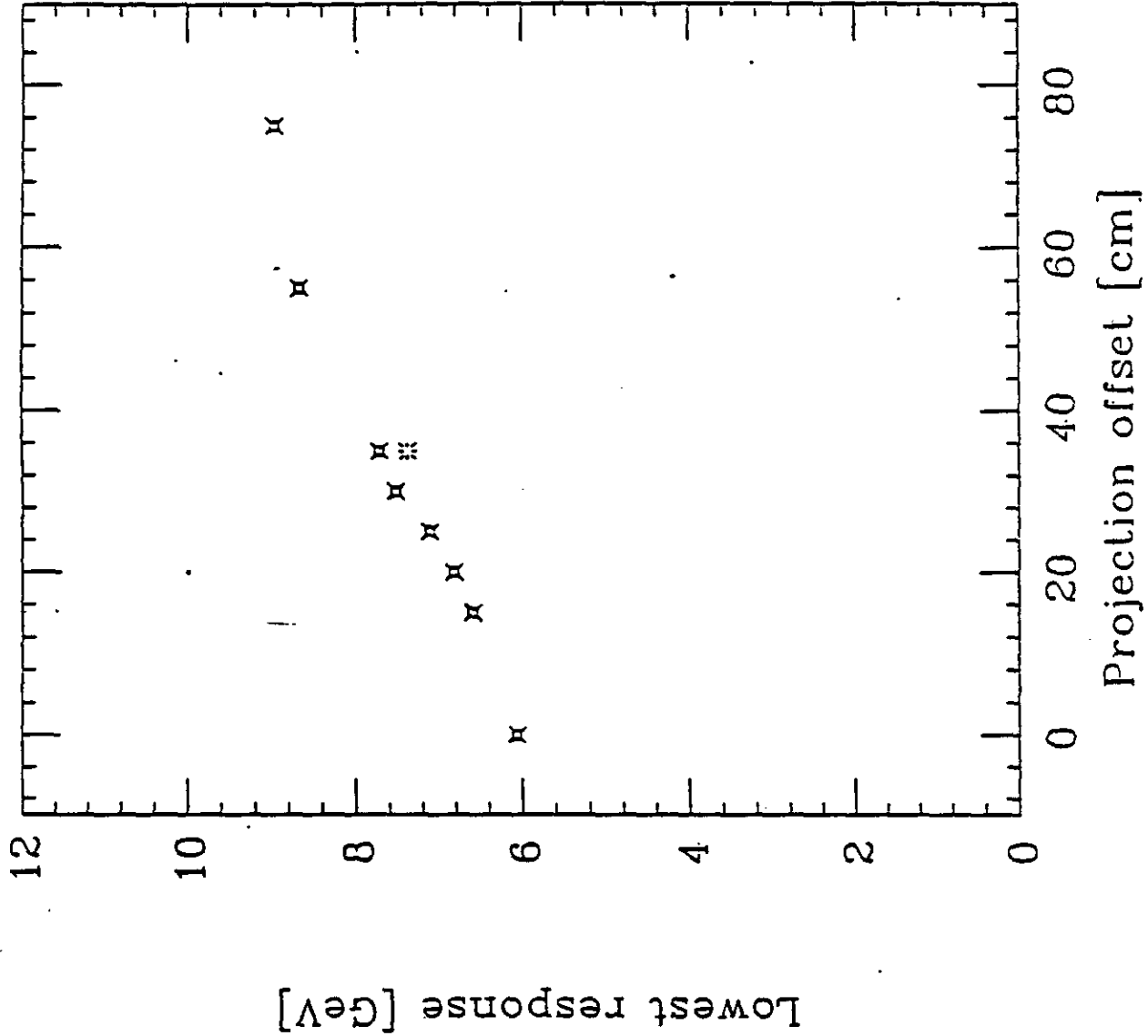
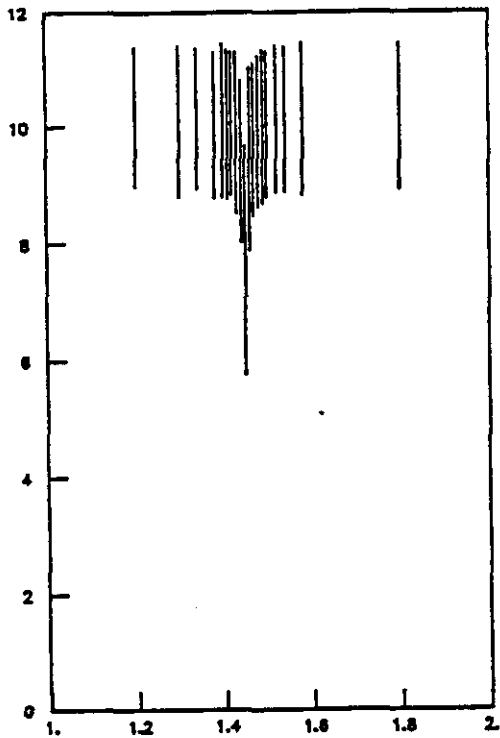
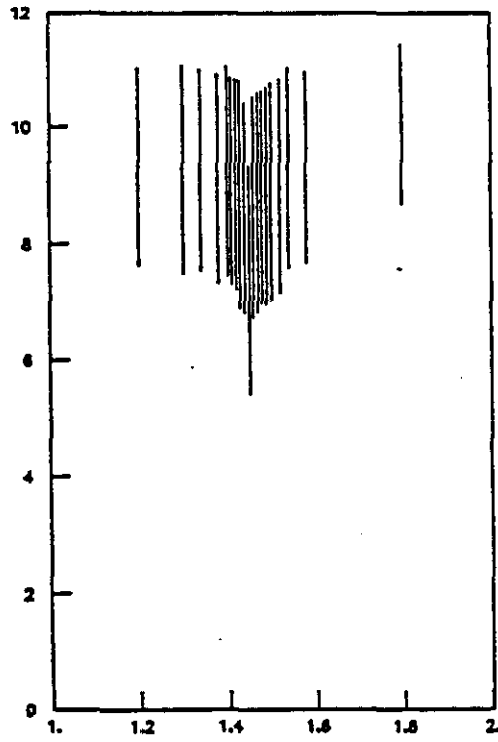


Fig. 4

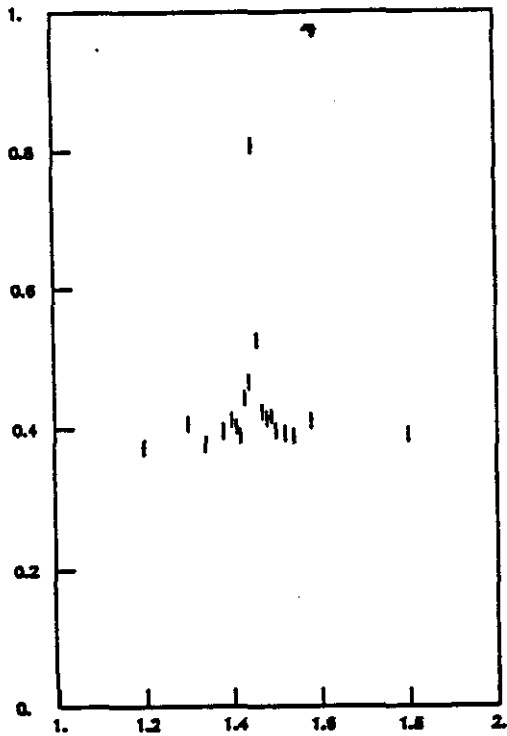
Calorimeter response over  $\eta$



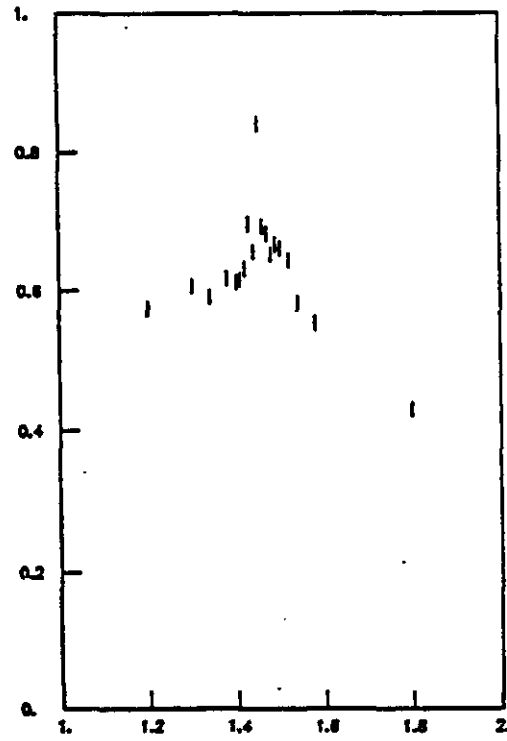
$\langle E_{cal} \rangle - \pi^-$ , offset 35 cm, no coil



$\langle E_{cal} \rangle - \pi^-$ , offset 35 cm, with coil



$\sigma_{cal} / \langle E_{cal} \rangle$  at 1 GeV -  $\pi^-$ , offset 35 cm, no coil



$\sigma_{cal} / \langle E_{cal} \rangle$  at 1 GeV -  $\pi^-$ , offset 35 cm, with coil

Fig. 5

Colorimeter response over  $\eta$

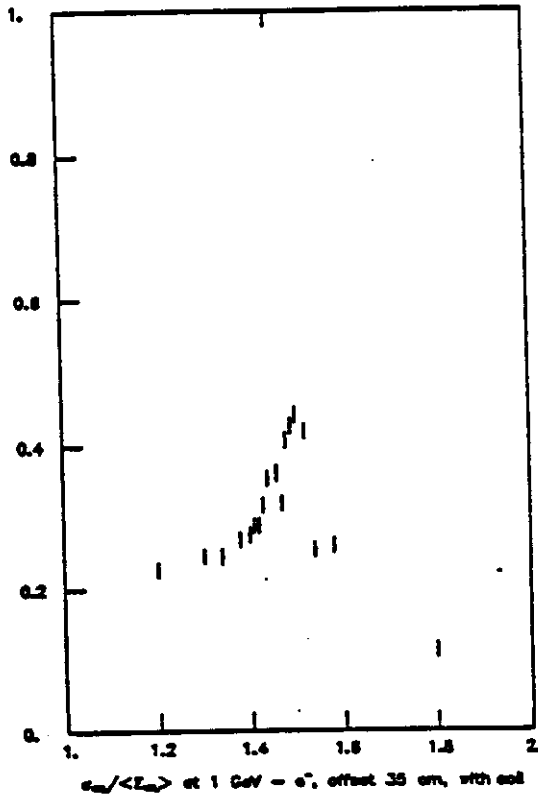
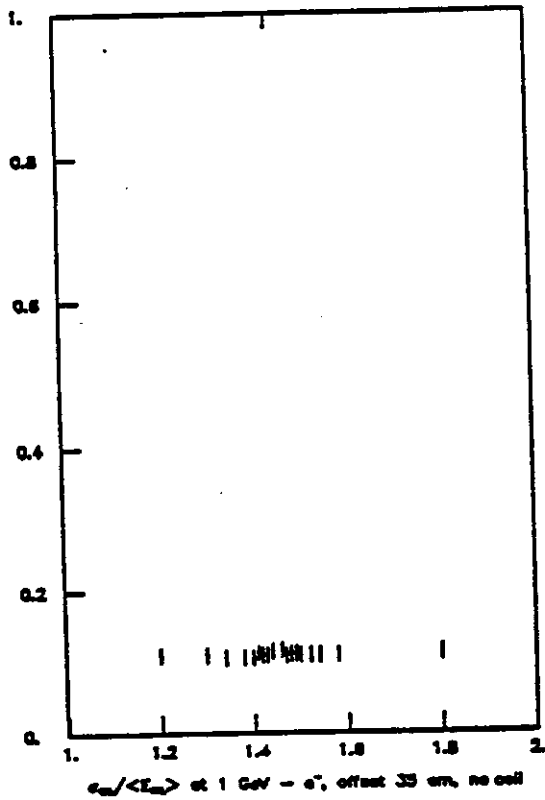
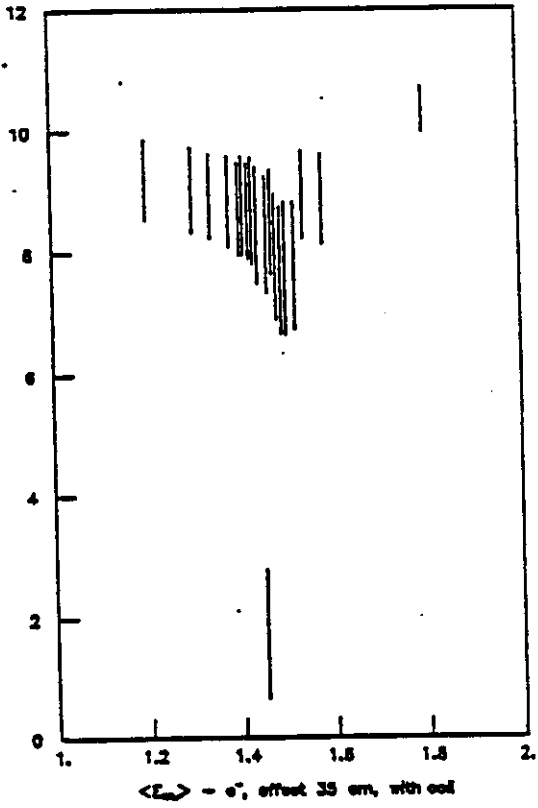
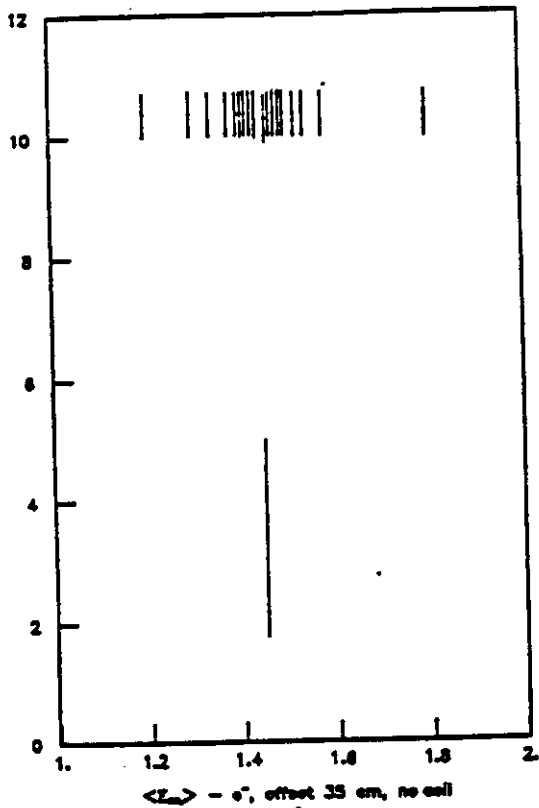


Fig. 6  
28

### APPENDIX III

#### REPORT ON RADIATION EXPOSURE OF LEAD-SCINTILLATOR STACK

D. Underwood

16 August 1990

A stack of lead and scintillator was placed in a neutral beam obtained from targeting 800 GeV protons. Small pieces of film containing radiochromic dye were placed adjacent to the layers of scintillator for the purpose of measuring the radiation dose to the scintillator. Our motivation was to calibrate the radiation dose obtainable in this manner for future tests of scintillator for SSC experiments. We also observed several other radiation effects which should be considered for an SSC calorimeter.

The lead-scintillator stack was constructed in a simplified manner due to limitations of space and materials. It consisted of CDF scintillator (5 mm) at 1/2 and 6 radiation lengths of lead, old scintillator from a prototype (5 mm) at 3 and 4.5 rad. len., Y7 waveshifter plate (3 mm) at 6 rad. len., and 1/2 rad. len. of lead behind. Dye film was placed at .5, 1.5, 3, 4.5, and 6 r.l.

The stack was placed at the face of the neutral beam dump of the polarized beam at Fermilab. The neutral beam is from very forward production and consists mainly of photons and neutrons. The collimator acceptance in the sweeping magnet is approximately  $\pm 0.7$  mr angle both horizontally and vertically. Approximately  $1.5 \text{ E}12$  primary beam was targeted per minute (on a 1 r.l. target) from July 26 to August 13 (18 days with about 30% down time). Approximately  $2.5 \text{ E}16$  protons were targeted. The order of magnitude neutral

beam we expected (gammas and neutrons) was one order of magnitude less than the number of primary protons.

The radiation exposure was determined by measuring the optical density of the radiochromic dye films with a spectrophotometer at two wavelengths. Calibration curves provided by Far Western Technology and traceable to NIST only covered .3 MRad to 2. MRad for 600 nm and .5 to 5. MRad for 510 nm. Curves for up to 100 MRad are published in a survey article on dosimetry.<sup>1</sup> The curve turns over at 50 MRad.

The dose was higher than expected and in a non-linear part of the response curve of the film. At .5 r.l. we found 8. MRad in the center and 1 to 2 MRad at the edges due to the beam profile. At 6 r.l. we found 40 MRad on the scintillator and 20 MRad on the waveshifter behind it. It is not known whether this difference is measurement variation or if the dose immediately behind the lead really is higher than behind 5 mm scintillator.

One possible problem with calibration of dose was possible exposure of the film to UV light from the scintillator excited by the particles in the electromagnetic shower. Possible light shields such as the garbage bag disintegrate. In fact, measurements between layers of lead with no scintillator were in reasonable agreement with measurements at the scintillator.

When the stack was removed from the beam, the induced radiation level in the lead at 6.5 rl was about 700 mR/hour on contact. The upstream side was about 200 mR/hour. The radiation was mainly gamma rays and had a half life of about 3 days. We believe that the isotopes responsible for the radiation can be determined. We are in the process of arranging for measurement of the gamma spectrum. Knowing the radiation history and the time constant, we could find the amount of induced radiation per primary proton, and using the

radiochromic dye to measure exposure, we could find induced radiation vs. radiation exposure. The induced activity is probably due to the neutron beam, but the hadron to photon ratio may be typical for hadronic reactions.

The steady state activity for constant rate exposure is the dose rate \* ratio factor \* decay time constant. Crudely, if we take 40 MR in 18 days and a time constant of 2.5 days, and .8 Rad activity, the ratio factor is  $1.6 \text{ E-}7$ . When the stack was disassembled after 2.3 days, the scintillator was found to have very little induced radiation (less than .005 of the lead).

When the stack was disassembled, there was radiation induced physical damage to plastic materials and paper. A thin dark plastic garbage bag disintegrated into small flakes. The paper on the CDF scintillator (the same paper used in the calorimeter) at 6 rl which was in contact with the lead turned to powder in the area of the beam, but the paper in contact with the scintillator was not as badly damaged. There was less obvious damage at 0.5 rl. Some white plastic foam used to cushion the older scintillator in compression with the lead disintegrated and stuck to the lead. The glue in stick-on paper labels used to attach the dye films became very hard and brittle. The CDF scintillator at 6 rl was yellow-brown but the others were transparent. The protective paper on the Y7 waveshifter surface had not been removed and became a white powder which was stuck to the surface.

This experience may aid in the future to make comparative measurements of the optical properties of damaged and undamaged stacks with the configuration of calorimeters. It would also be interesting to relate the dose to the photon and neutron flux if these could be determined adequately.

#### ACKNOWLEDGEMENTS

We thank J. Sheppard of ANL HEP for help with the lead, the Fermilab Radiation Safety section for help with activity measurements, M. and J. Peak of ANL BIM for help with the spectrophotometer, and W. McLaughlin of NTIS for help in finding calibration information.

#### REFERENCES

- 1) MEGAGRAYS DOSIMETRY, W.L. McLaughlin et. al., Radiation Physics and Chemistry, Vol. 22, p. 33 (1983).

## FLASH ADC TESTING

H. B. Crawley, W. T. Meyer, E. I. Rosenberg, W. D. Thomas

Ames Laboratory, Iowa State University

Ames, Iowa

The Ames Laboratory/Iowa State University group has developed a CAMAC-based test bench along with appropriate software for the evaluation of commercially available Flash-ADCs capable of digitizing signals every 16 nsec. A VAXstation 3100 running VMS controls and monitors the test bench. Communication between the computer and the test equipment utilizes a SCSI bus, a SCSI to GPIB interface which allows communication with both a function generator and a signal generator, and a SCSI to CAMAC crate controller. Two special purpose CAMAC boards have been built to evaluate the FADC performance. The function and signal generators provide input to these CAMAC boards, and a digital oscilloscope is also connected via the GPIB bus. The two programmable CAMAC boards provide clock and trigger signals, and interface to various FADC evaluation boards (usually supplied by the manufacturer). The clock/trigger board allows ten discrete clock frequencies in the range 20 - 140 MHz to be supplied to the FADCs. Extension to lower values in order to allow the testing to devices with dynamic ranges wider than those currently available at high sampling frequencies is possible. The FADC interface board contains 1-kbyte of fast memory to store digitized data. Our tests follow the guidelines given in IEEE Std-1057, "IEEE Trial-use Standard for Digitizing Waveform Recorders". The gain and offset are determined statically using a

series of dc levels and dynamically using a single sine wave input. The differential nonlinearity is determined statically using dc levels and dynamically using a triangular signal input. Programmable dc levels are also used to calculate the integral linearity, maximum static error, monotonicity and hysteresis. The effective number of digitizing bits, signal-to-noise ratio and peak error are determined using a single sine wave input. Multiple sine wave inputs are used to determine the analog input bandwidth of the digitizer as well as the aperture uncertainty. Long- and short-term settling times are determined using a step function input. Random noise and the word error rate are determined using the triangle wave input. We also measure the slew limit and absolute overvoltage recovery. As of August 27, both specialized boards have been built and are undergoing final debugging. The software has all been written and partially tested. Testing of specific Flash ADCs from Analog Devices, Datel, Siemens and SONY will begin in September. Initial results are to be presented at the Fort Worth meeting and at the Nuclear Science Symposium of the IEEE in October.

## SUMMARY OF LSU WORK ON OPTICAL SYSTEM

A. Fasely, R. Imlay, R. McNeil, W. Metcalf

Louisiana State University

The work proposed by LSU is in regard to the optical system of the calorimeter. We must ensure an adequate efficiency in the coupling of the scintillator light via a waveshifter plate and light guide to the photon detector so that the photon statistics will not dominate the resolution. The physicists from LSU who have worked on the project are R. Imlay (25%), R. McNeil (25%), and W. Metcalf (15%). Their amount in percentage reflects the fraction of their research time to be devoted to the tasks. An additional Research Physicist, A. Fasely has recently joined the effort and will work half-time on this project in FY91. In addition we will require the technical support equivalent to 1 full-time technician. The main tasks assigned are:

- 1) Evaluate the optical performance of radiation exposed scintillator and wavelength shifter material to determine the light transmission, light output, and radiation damage recovery. This will be for tiles of the size of cells on the proposed calorimeter. The greatest radiation damage will occur in the EM portion of the calorimeter. LSU will wrap  $10\text{cm} \times 10\text{cm}$  laser-cut tiles of various thicknesses and materials produced at BICRON Inc., and measure their overall light yield and uniformity. The tiles will then be exposed with an intense source at ANL or electron beam at FSU and the damage (loss of output and uniformity) will be recorded during (or immediately after) exposure. The damage recovery will be

monitored back at LSU with our test facility. The designated manager for the task is R. McNeil.

- 2) Measure the light detection efficiency. Measure the system efficiency of the optical design proposed for the calorimeter (scintillator, waveshifter plate or fiber, lightguide, and photon detector). LSU will investigate the coupling of scintillator tiles to WLS plates, and WLS fibers. Light output performance and uniformity will be evaluated for different readout designs. Individual tiles will be measured at LSU. The designated manager for the task is R. McNeil.
- 3) Optimize the optical structure. Determine the structure of filters and reflectors required to obtain the necessary detector uniformity consistent with the chosen optical geometry. Optimize the structure to maximize the light yields. For WLS plate readout, reflection masks will be prepared using the results of the measurements of the individual scintillator tiles and the WLS shifter plates. The method employed by LSU to prepare the ZEUS EMC WLS reflection mask will be adapted to this case. For WLS fiber readout, reflection masks can be attached directly to the scintillator tiles provided the correction required is not too large. LSU will investigate this. The designated manager for the task is R. McNeil.

#### Summary of Work Performed as of September 1, 1990

LSU received its first scintillator from Bicron. On August 15, 1990, 15 scintillation tiles 10cm \* 10cm \* 2.5mm thick and some WLS fiber were received. The effort this summer has concentrated on the preparation of a scintillator tile test station with an beta source. This consists of a computer controlled scan table (see Fig. 1). The scan table will be utilized to perform initial measurements of scintillator tiles and long term aging and

recovery studies on the tiles.

The plan for the following month (September, 1990):

- 1) Wrap and measure the 15 scintillator tiles received from Bicron. Expose a subset of the tiles in an electron beam (at FSU) or with a neutron source (at LSU) to expected SSC radiation dose levels and determine the initial damage to the optical performance and the recovery characteristics of the system.
- 2) Determine a suitable method to attach WLS fiber to tiles. Evaluate the relative performance of the scintillator tiles read out via WLS plates vs WLS fibers in terms of overall light yield and uniformity. Determine a means to correct for non-uniformity for each readout option. Expose some of the completed scintillator tile/WLS fiber as above and determine the initial damage to the optical performance and the recovery characteristics of the system.
- 3) Measurement of WLS pipe attenuation length and radiation damage. 10cm \* 1m (or 2m) Wave-Shifter plates will be cast at Bicron and shipped to LSU where they will be measured using our ZEUS WLS plate scan table with a UV lamp. The pipes will then be exposed in an electron beam (at FSU) or neutron source (at LSU) and the light yield and uniformity re-measured. Long term recovery of the WLS plate will be studied at LSU.

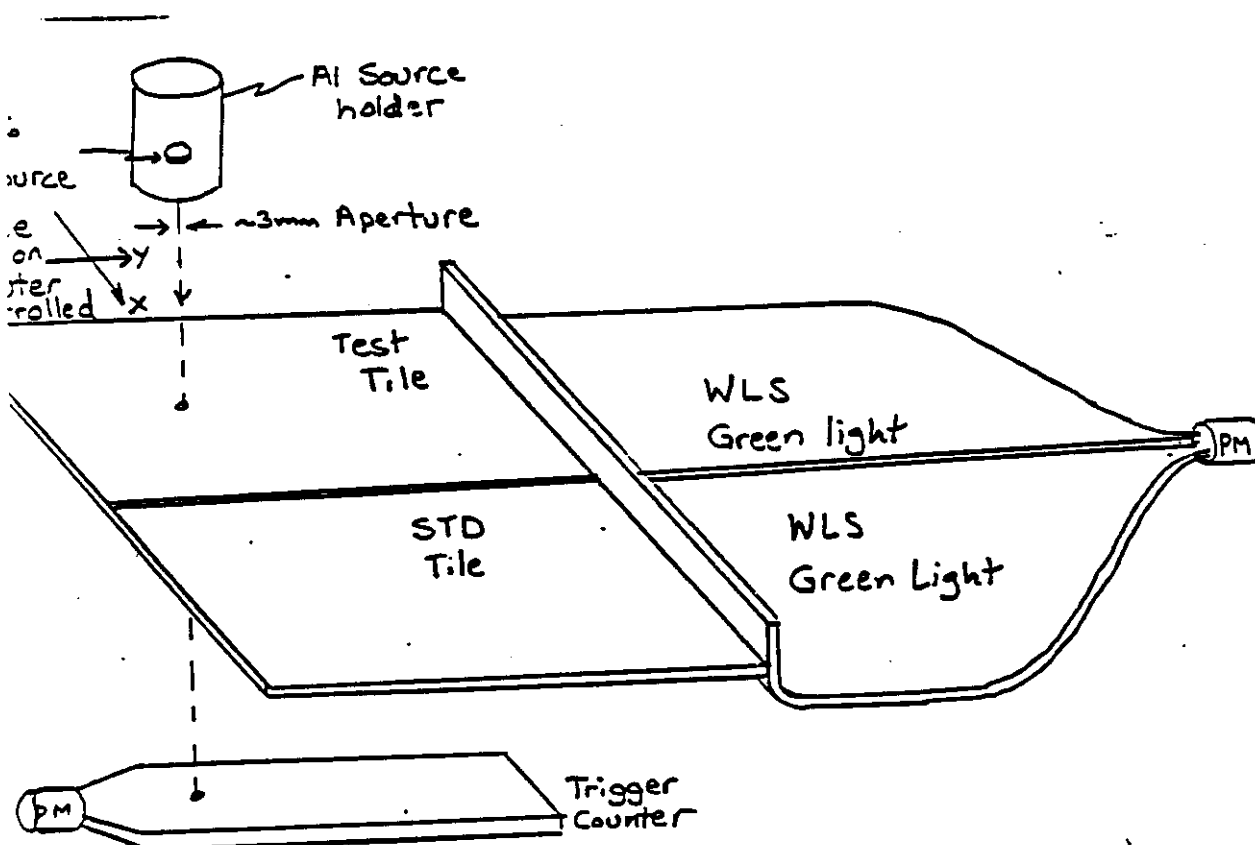


Figure 1

FLORIDA STATE UNIVERSITY

RADIATION DAMAGE STUDIES OF SCINTILLATORS AND WAVE SHIFTERS

(Progress Report -- August 1990)

M. Bertoldi, M. Goforth, V. Hagopian, K. Hu, K. Johnson, P. Rulon,  
J. Thomaston, K. Thomson, H. Wahl, H. Whitaker, J. Xu, A. Young

ABSTRACT

The Florida State University group consisting of 12 persons investigated the radiation hardness of various plastic scintillators and scintillating fibers. Two major successes are: the newer scintillator from BICRON which is an order of magnitude more radiation hard than previous materials. Second: the use of 3HF first suggested by an FSU Bio-Physicist as a better wave shifter.

Our group hosted an international workshop on radiation hard scintillators in March 1990, where the latest knowledge was reviewed and goals defined for scintillators to be useful at the SSC.

We will now describe in some detail our work on measuring and helping develop new and more radiation hard scintillators.

Plastic scintillating fiber is a serious candidate to be the active tracking medium at the SSC because of its triggerability and speed. Plastic scintillator in plate form with either plate wave shifter or fiber wave shifter is a leading contender to be the active medium for the barrel calorimetry at the SSC, both because of its speed and its ability to achieve compensation without uranium. Both applications critically depend on the ability of the active medium to receive large doses of radiation without degrading instrument performance to an unacceptable degree.

In November 1988, Florida State University and the University of Florida initiated a collaboration to investigate radiation damage to plastic scintillator. The collaboration, which lasted until December, 1989, was very successful. We developed techniques for controlled irradiation at the FSU 3-MeV electron linac and did comparative studies of the radiation resistance of scintillating fibers as well as composition and temperature effect studies. These results were reported at the Tuscaloosa Workshop on Calorimetry for the SSC, March 1989, at the Berkeley Meeting on the Radiation Survivability of Scintillating Calorimeters, July 1989, Berkeley, California, (SSC-N-650), and in a Nuclear Instruments and Methods article [A281(1989)500-507].

Radiation damage manifests itself as a decrease in the attenuation length and a decrease in the local light yield. Our fiber investigations have led to partial remedies to both problems. The first fruitful result was the demonstration that the use of a large Stokes' shift fluor results in tremendous advantages, namely, a tenfold increase in radiation hardness and very long attenuation lengths. 3-HF, the first such fluor to be used, was originally investigated by FSU chemists. Its use as a fluor and the expected advantages to be accrued were first suggested by S. Majewski, who recognized that utilizing long wavelengths would by-pass color centers in a damaged plastic base, thus ameliorating the radiation induced decrease in attenuation length. (This is sometimes called the "better red than dead" strategy.) A partial remedy to the problem of a decrease in local light yield is to increase the concentration of the secondary fluor by a factor of 10 to 100. With most fluors this will result in very short attenuation lengths due to the re-absorption of emitted light. In the case of a large Stokes' shift fluor such as 3-HF, however, the re-absorption of emitted light is almost nil, and this technique suddenly becomes a viable option. First results were published

in the IEEE Transactions on Nuclear Science (Vol. 37, No. 2, April 1990) showing only a 33% light yield loss after an exposure of 100 Mrad. This is an enormous improvement over previous performance.

We are now engaged in a thorough and systematic investigation of local light yield, attenuation length and damagability as a function of 3-HF concentration.

A second area of investigation is the damage to the plastic base. Results produced by the FSU/UF collaboration proved that modifications to polystyrene base plastic could "harden" the base by an order of magnitude. BICRON Corporation, motivated by these results, has recently created an improved base material, designated RH-1, which we are now testing.

Much effort on the past half year has been expended on improving the precision and quality of our data. We can now irradiate even long fibers (>2.5 meter length) to any reasonable dose with extreme uniformity. Dosimetry is non-trivial for low energy electron beams, but we have refined our procedures so that we can measure the absolute dose given to a test object to an error of 7%.

The immediate gas and chemical environment is of fundamental importance in both the severity of damage caused and the recovery therefrom. Scintillating plastic which is embedded inside a calorimeter or epoxied to the mechanical support of a fiber tracker will be affected differently than scintillator which has unrestricted access to air. To investigate these phenomena, FSU initiated a collaboration with the University of Illinois at Urbana-Champaign to build fiber calorimeters with advanced, radiation resistant materials and test them at the UIUC 100 MeV electron Microtron. Modules fabricated from an especially designed PTP/3-HF/PS fiber and from the new experimental radiation hard base material RH-1 have been built and are currently being tested.

Results have been presented at the ECFA Study Week on High Luminosity Hadron Colliders, September, 1989, Barcelona, Spain, and published in the IEEE NSS Proceedings and in the Proceedings of the Workshop on Radiation Hardness of Plastic Scintillator, March 1990, Tallahassee, Florida. A Nuclear Instruments and Methods paper is now in preparation.

FSU has also been active in both coordinating research and in disseminating the results. In March, FSU together with FERMILAB hosted a Workshop in Tallahassee on "Radiation Hardness of Plastic Scintillator". The Proceedings will be printed and distributed by August. The Workshop proved to be instrumental in focusing attention on critical problems.

One month ago we received the first sample of scintillating plates made of RH-1. We now have radiated these samples with radiation of 0.1, 0.3, 1.0, 3.0 and 10. Mrad. All have various amounts of damage but recovering very rapidly. So far in three weeks all plate scintillators with radiation of one Megarad and lower have completely recovered, with no loss of light emission with 1% accuracy. The 3 and 10 Megarad samples are still recovering. Since we have had fibers for a longer period, we will summarise below our results of some of these fibers.

9 Aug. 1990

Summary of Radiation Damage of Fibers

<u>Fiber</u>	<u>Attn Length Undamaged</u>	<u>Attn Length No Recovery</u>	<u>Attn Length After Recovery</u>	<u>Light Loss No Recovery</u>	<u>Light Loss After Recovery</u>
BC048 10 Mrad Blue				50%	25%
3HF Bicon 10 Mrad Green	190 cm	< 10 cm	30 cm	35%	25%
Optectron 10 Mrad Blue	200 cm	< 5 cm	12 cm		
SCSN81+Y7 3 Mrad Green	250 cm	< 5 cm	62 cm	25%	9%
SCSN81+Y7 1.2 Mrad Green	250 cm	< 33 cm	95 cm	7%	2%
Bicon G (3HF) 3 Mrad Green	190 cm	< 10 cm	167 cm	12%	8%
Bicon RH1 10 Mrad Blue	235 cm	< 22 cm	60 cm	17%	8%
Bicon RH1 3 Mrad Blue	235 cm	< 40 cm	75 cm	13%	3%
Bicon RH1 1.2 Mrad Blue	235 cm	< 81 cm	100 cm	8%	1.6%

## Virginia Polytechnic Institute

J. R. Ficenece, B. Lu, L. Mo, L. E. Piilonen, T. Nunamaker

### 1) Monte Carlo Simulations

Virginia Tech, a member of the ZEUS collaboration, has a full GEANT simulation program for that experiment running on the supercomputer, C210 made by Convex, of the Institute of High Energy Physics at Virginia Tech. The hadronic, and in particular the neutron, interactions in this program have been done correctly to deal with the uranium and scintillator calorimeter. To date, this program has been used to study hermeticity in the uranium/scintillator calorimeter concept. We plan to modify this code to properly treat the lead/scintillator system and to continue the hermeticity studies of the calorimeter under design. The request of support pays a fraction of the computer maintenance contract.

### 2) Photon Detector

The proposed calorimeter has between 40K and 50K individual channels, and the first step in the signal processing is to turn the light coming from the scintillator and wavelength shifter into an electrical pulse by means of a photon-charge transducer. A dynamic range of  $\sim 10^5$  to 1 is required with good linearity and the device must obviously be reliable and stable in operation over long periods of time. There are two practical ways to proceed:

## 2.1 Photomultiplier Tube (PMT)

The conventional way of doing this job is through the use of photomultiplier tubes. The scintillation light is directed onto the photocathode through a wavelength shifter fiber (or bar) and lightguide. The ejected photoelectrons are amplified by the dynode structures with a gain of  $\sim 3$  at each dynode. After ten or more stages of amplification, large pulses become available at the anode and the last dynode. Even though this technique is mature and well understood, it has some shortcomings. In particular, the PMT and its high voltage base are bulky and not tolerant of magnetic fields.

If PMT's are to be used in the proposed calorimeter, then they should be of small size ( $\leq 1.5$ " dia.) and have high gain. A 10-stage tube, such as the R580 tube made by Hamamatsu of Japan, would be suitable. This tube has a dynamic range corresponding to a peak pulse of  $\sim 160$  ma into a  $50 \Omega$  load impedance. For experiments at the SSC, it is desirable to miniaturize the tube further.

The conventional high voltage bases, made of resistors, capacitors, and Zener diodes, are not suitable for this calorimeter since they generate too much heat (1 to 2 watts per base). The high voltage cables are also too heavy and bulky. A large number of high voltage cables are difficult to bring out of the detector without creating holes, and they could also provide serious fire hazards. For the ZEUS experiment, an elegant "Cockroft-Walton" accelerator type base has been developed by the Virginia Tech group, in which the high voltage is locally generated within each individual base. This solution is also suitable for an SSC calorimeter based on scintillator with PMT readout. Moreover, this type of base produces only about 0.15 watts of heat per channel. A 100 kHz oscillator in the base is energized by a DC source of 24 volts, and the rf output is raised to  $\sim 120$  volts by a small

ferrite transformer. A Cockroft-Walton chain, made of capacitors and rectifiers, is then powered by this rf to produce the desired high voltage for the PMT. The stability of the high voltage is maintained to within  $\pm 0.3$  volts by an analog feedback loop. The noise level in the anode outputs is  $\sim 0.020$  pC, which is comparable to that of the conventional resistive tube bases.

The high voltage controller used with these bases are VME bus devices. They have local intelligence, software in EPROM's, ADC's, Ethernet, and R5232 communication ports. Each individual base plugs into the controller through a flat ribbon cable, which carries the low voltage DC power and control signals to the base. This system will work for the proposed SSC calorimeter without significant modifications, although we expect to use up-to-date processors and optical fibers as the communication channel for the final calorimeter.

We have been financed by the Department of Energy to procure the photomultiplier tubes, bases and high voltage controllers for the electromagnetic part of the prototype calorimeter. They will be tested at Fermilab in 1991 and the results provided to this collaboration for use in evaluating the suitability of this option.

## 2.2 Hybrid Photomultiplier Tube (HPMT)

Very recently, we received a brand new prototype of "hybrid photomultiplier tube". This device looks externally very much like a conventional PMT. It is encased in a glass enclosure and its mechanical construction is quite sturdy. The physical dimension measured 1.75" in diameter, and 1.75" in length.

In a HPMT, the photo-electrons from the cathode are accelerated to 15 KeV and focussed onto a silicon solid-state detector. Since it takes  $\sim 3.62$  eV to

produce an electron-hole pair in silicon and both charges are collected, the device has a gain of  $\sim 10^4$ . Preliminary testing results indicated that:

- The response over the whole photo-cathode surface is uniform. Perhaps this is not surprising because the device is an evolution of a high quality image intensifier unit.
- The output signal from the silicon detector of the HPMT is very fast. It has a rise-time of  $\sim 2.5$  nsec, a fall-time of  $\sim 5$  nsec, and a full-width at half-maximum,  $\sim 5.5$  nsec.
- The spectral response is good at wavelength of 400 to 550 nm.
- The output signal begins to show non-linearity at  $\sim 23$  mm while the noise is of the order of 10 nano-amp.

It appears to us that this HPMT is a promising candidate to replace the photomultiplier tubes in SSC calorimeter applications because of its compact size and its single-stage high voltage distribution. Further R&D effort would certainly be most beneficial to the whole physics community at large. In FY1991, we request support from both TNRLC and DOE to finance the following tasks:

- 1) To develop a fast charge-sensitive amplifier to handle the 16 nsec beam crossing-time requirement of SSC.
- 2) To develop a compact size, computer controlled 15 kV power supply. Since there is very little power requirement, we can employ the Cockcroft-Walton technology.
- 3) To continue the detailed measurements with this HPMT. We would like to learn more about its long term stability, dynamic range, spectral response, radiation resistance and operating characteristics.

- 4) To negotiate a reasonable price to purchase - 20 units, and to suggest possible improvements in both performance and price for future quantity production if this device is adopted.

It is our hope that we can install these HPMT's on the prototype electromagnetic calorimeter and have the whole system beam-tested at Fermilab in early 1991. As mentioned earlier, one set of R580 photomultiplier tubes have been prepared for the fall-back position.

W. Smith

## SUBSYSTEM ELECTRONICS ACTIVITIES UNIVERSITY OF WISCONSIN PROGRESS REPORT

The electronics effort of the scintillation detector subsystem is proceeding in two stages. The first stage is to equip a test-module with commercially available electronics to measure the performance of the module and to establish a reference point for comparison with the eventual custom electronics. It is also planned to incorporate a realistic shaping filter and analog memory unit. The test-module will be composed of a 5x3 cell matrix. A total of 15 calorimeter cells will be available for instrumentation. The test-module will be inserted into a test beam early in 1991. The electronics preparations for this test are now seriously delayed due to lack of receipt of approved funding.

It is anticipated that tests of the electronics will be carried out before the test beam run on a test bench. Here we plan to expose a scintillator to short pulses of  $uv$  light which would simulate excitation of the primary fluor with shower particles. The  $uv$  pulses would be no longer than 10 nsec long; this allows the natural decay times of the primary and secondary fluors to dominate the scintillation process and thereby to simulate electromagnetic showers.

The work thus far has concentrated on the following activities by the University of Wisconsin.

- Phototransducer: We require a fast, commercially available photomultiplier. A large number of photomultipliers were evaluated for use in the beam test. Hamamatsu, Phillips, Thorn-EMI, Burle and EMR firms responded to requests for specifications. Based on the results of evaluation of these responses the Hamamatsu R-580 was chosen for use in the beam test.
- Base and preamplifier: It has been decided for reasons of scheduling to proceed with acquisition of a standard resistive base designed for fast signal generation. The conceptual design of this system is underway and awaits funding for engineering.

- Current Divider Pulse Stretcher (55 ns max) and Amplifiers: The PMT output will be divided among several systems. The dynamic range necessary leads to inclusion of both low and high gain channels. A trigger signal must be developed and, if DU is used, the DU noise signal will be used for calibration. The signals, shaped as needed, will be sent to three read-out systems (backup LeCroy, LBL-based memory chip, and rad-hard memory chip). The conceptual design of this system is underway and awaits funding for engineering.

For the base, preamplifier, current divider, pulse stretcher and amplifiers, the conceptual designs for these devices have been developed on the basis of the following specifications:

The Test Calorimeter have 15 channels total.

The phototube diameter will be 1" - 1.5".

Two ranges will be used with 8000:1 each. The high gain range will be set to place a mip in channel 100. The low gain range will operate up to 400 GeV.

The time resolution will be less than 1 nsec (already achieved in Zeus).

The sampling rate will be 18.8 nsec (FNAL RF structure, which is close enough to SSC 16 nsec).

The data rate will be greater than 100 events/second.

The time constant of the shaping will be about 3 times the sampling time, or 54 nsec.

About 1/2 of the current from the PMT will be diverted from the standard measuring system to a second output for electronics studies.

There will be charge injection.

The length of the pipeline (time over which samples are stored) will be 1 usec.

We will use need a laser to test the system since this is the only way to cover the dynamic range to check linearity.

The initial conceptual design has resulted in the following plans:

We will use as our principal system a "LeCroy" ADC system. We will build 3 channels or so (enough for one tower) of two experimental systems to be available on January 1991. We may continue and build a full 27 channels of one experimental system to instrument the entire prototype before the test beam turns off.

The preamplifier, current divider shaper/pulse stretcher and amplifier circuit board will be designed and built by the Wisconsin group. Some of the circuitry may be mounted in the base (e.g. preamplifier).

In collaboration with Ames Laboratory, we plan to:

- Install and test a readout system employing the LeCroy ADC to study pulse shape and as backup for analog memory (Some units already in hand, more to be obtained). The Wisconsin group has specifications on the LeCroy 2249, 2280, and 4300 ADC systems and has experience with each. The most likely system to be used will be the LeCroy 2260 system which is based on the MVV200 CCD. The Wisconsin group has experience with the MVV200 since it was used for the initial Zeus readout. The Ames group has experience with the 2260 series system.

In collaboration with Westinghouse Corporation and the Front End Electronics Subsystem we plan to:

- Incorporate electronics provided by "front-end" subsystem group in prototype testing (shaper/amplifier, analog memory, ...) Discussions have taken place with the Front End Electronics group and the Subsystem Electronics group. A plan of joint cooperation has been developed whereby the analog pipeline from the Front End Electronics group will be tested with preamplifier electronics from the subsystem and an am-

plifier either from the subsystem or the Front End Electronics group. This will be done using the additional electronics channel as specified above. Westinghouse will collaborate on the driving and readout system for the analog pipeline.

Progress Report  
for  
The Scintillating Plate Calorimeter  
Subsystem

T. Handler\*  
Physics Dept.  
Univ. of Tennessee  
Knoxville, Tennessee 37996-1200

J. Reidy, L. Cremaldi  
Physics Dept.  
Univ. of Mississippi  
University, Mississippi 38677

R. G. Alsmiller, Jr., C. Y. Fu, and T. A. Gabriel\*  
Oak Ridge National Laboratory  
P. O. Box 2008  
Oak Ridge, Tennessee 37831-6364

### ABSTRACT

During the past year, Tennessee, Mississippi, and Oak Ridge National Laboratory have been coordinating efforts to benchmark the CALOR89 code system against the ZEUS prototype calorimeter data, and to use the CALOR89 system to generate currently needed data for radiation damage studies, signal collection time, and compensation characteristics of various calorimeter designs. This report describes these results and gives our plans and projected budgets for the following year.

#### I Introduction

A strong experimental Superconducting Super Collider (SSC) calorimeter development program must involve a substantial calculational analysis of the proposed detector system. The CALOR89<sup>1</sup> code system offers a solid approach for investigating all facets of calorimeter systems. Due to financial constraints, only a few prototypes can be built and tested. The remainder of the studies must be analytical. Once the calculated results have been shown to agree with the test data, a much wider variation of the design can be investigated. This approach is being followed in our subsystem research.

During the past year, Tennessee, Mississippi, and Oak Ridge National Laboratory have been coordinating efforts to benchmark the CALOR89 code system against the ZEUS<sup>2</sup> prototype calorimeter data, and to use the CALOR89 system to generate currently needed data for radiation damage studies, signal collection time, and compensation characteristics of various calorimeter designs. Even though the total benchmarking of the ZEUS data has not been completed, the current caliber of the code is such that data generated will certainly be adequate for preliminary design studies. This report describes these results and gives our plans and projected budgets for the following year.

---

\*Coordinators

## II. The CALORS9 Code System

A flow diagram of the CALORS9 code system is given in Fig. 1. The transport codes that comprise this system include HETCSS<sup>3</sup>, the high energy hadronic transport code, EGS4<sup>4</sup>, the electron, positron, and gamma ray transport code, MORSE<sup>5</sup> and MICAP<sup>6</sup>, the low energy ( $\leq 20\text{MeV}$ ) neutron transport codes. Source gamma rays and electrons for EGS4 and neutrons for MORSE are obtained from the data generated in HETCSS. The remainder of the codes are for analysis (SPECT and ANALYSIS), cross-section generation (PEGS), and signal reduction due to saturation/recombination effects (LIGHT). The major changes in CALOR and the main reasons for the additional benchmarking are an improved high energy collision model following the methods used in FLUKAS<sup>7</sup> and a new low energy neutron transport code, MICAP. To prevent too many changes at once, the code will be benchmarked against the new high energy model using the MORSE code and will be followed by additional benchmarking using the MICAP code.

## III. Signal Collection Time and Compensation Characteristics of a Pb/Scintillator Calorimeter

The configuration of the calorimeters considered in these calculations are given in Table I. In both cases, the scintillator has been kept at a thickness of 1mm while the lead thickness is varied from 4 to 3mm. The lateral width of both detectors is  $2 \times 2\text{m}^2$ . The total thickness in the 3mm Pb calorimeter case is slightly larger, but should not grossly affect the comparison between these two systems. There should be slightly less leakage in the 3mm system.

Presented in Fig. 2 are the pulse heights calculated for 10GeV electrons, protons, and pions incident on the 4mm Pb/1mm Plastic calorimeter. The histogram is the actual calculated data and the solid curves represent the fitted Gaussian distributions. All quoted  $e/\pi$  ratios and resolutions are obtained using the fitted data.

The effect of saturation and time cuts on the compensation characteristics of a plastic calorimeter are rather strong. Presented in Fig. 3 are compensation results as a function of time and saturation level for the 4mm Pb/1mm (4,1) Plastic calorimeter for 10 GeV incident protons and pions. As can be determined, the calorimeter would be substantially over compensating if saturation was not present in the plastic scintillation. This important parameter is often neglected when various plastics are considered for the calorimeter. Also as can be seen in this figure, approximately 50-75nsec is required to collect most of the signal and to obtain compensation. Similar data for both calorimeters (3mm (3.1) and 4mm (4,1) Pb) and various particle energies are presented in Fig. 4. Odd fluctuations in the location of the data curves are attributed to back leakage.

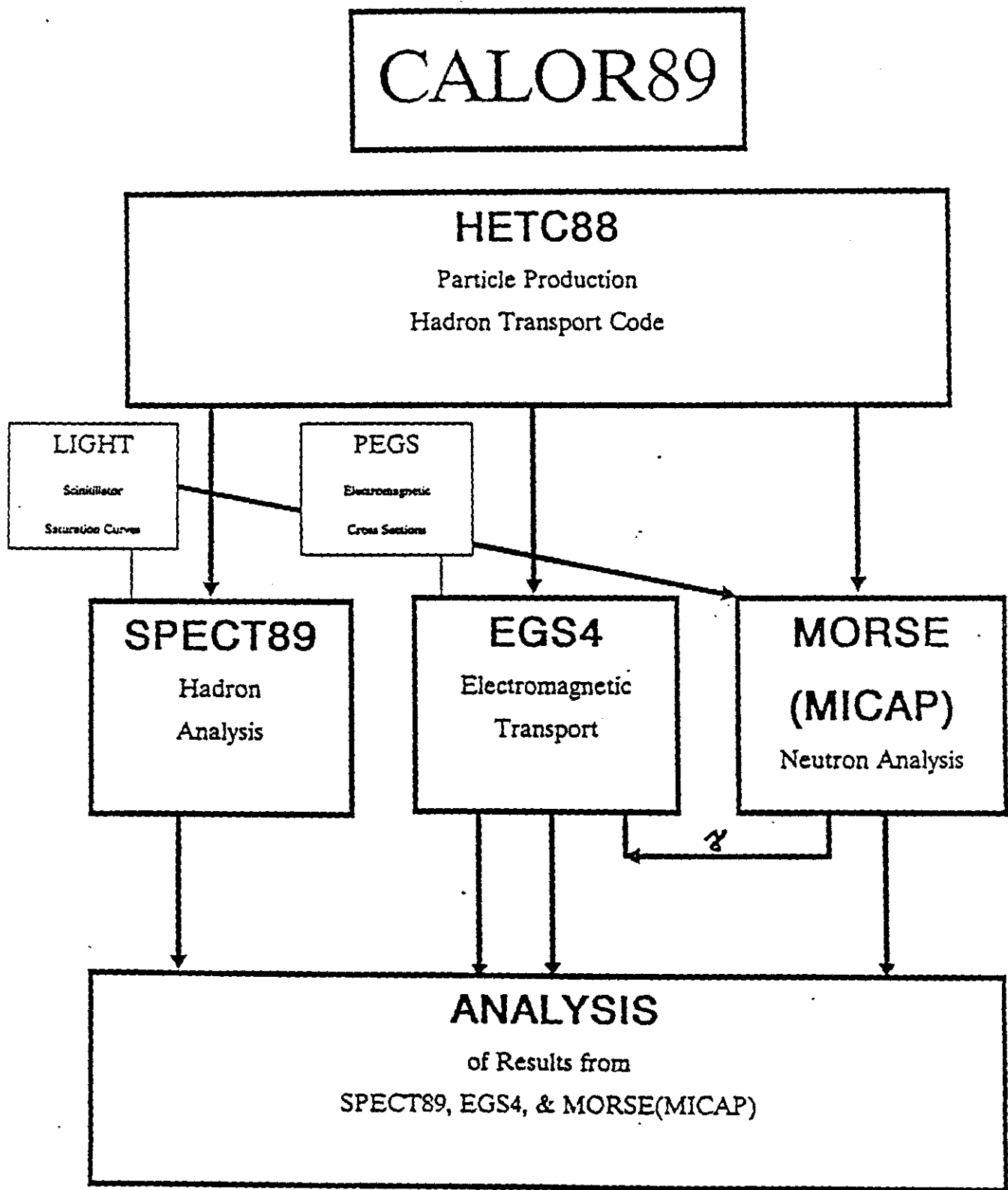


Fig. 1 The CALOR89 Code System

## Table I

### Geometry of the Lead-Scintillator

#### Calorimeters

##### 4mm Pb, 1mm Sci

- Total depth - 150cm
- 300 Samplings
- 7.02 Interaction lengths of Lead

##### 3mm Pb, 1mm Sci

- Total depth - 160cm
- 400 Samplings
- 7.02 Interaction lengths of Lead

The resolution as a function of cutoff times, particle energies, and calorimeters is presented in Fig. 5. The data have been fitted to

$$\sigma/E = A/\sqrt{E} ,$$

and the A value plotted. Due to back leakage the resolution becomes slightly larger at 20 GeV. Also due to less compensation for the 3mm/1mm calorimeter case, generally speaking, the resolution will be worse and a constant term should be added to the equation, i.e.,  $\sigma/E = A/\sqrt{E} + B$ , before fitting.

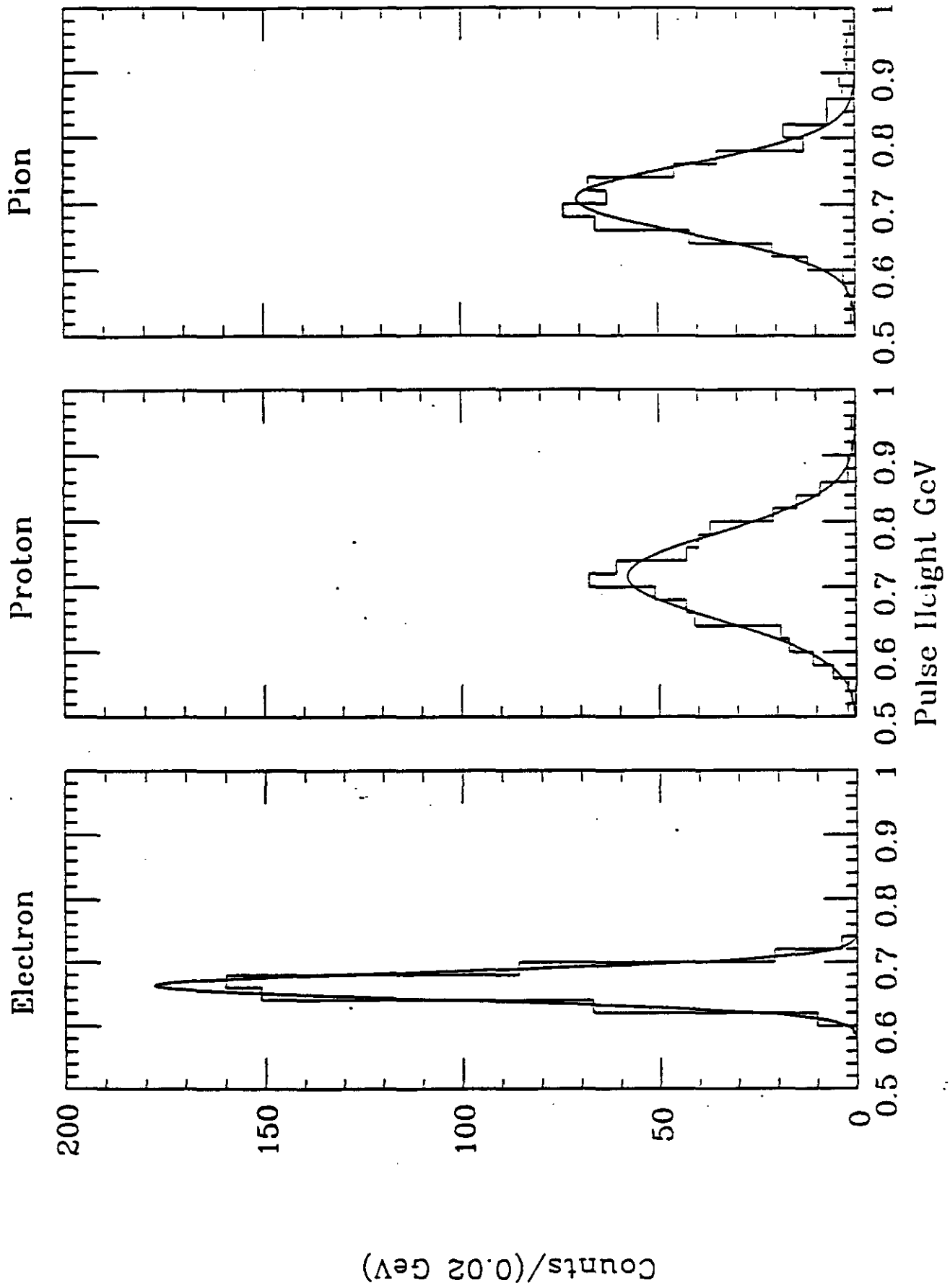


Fig. 2 Pulse height distributions for 10 GeV electrons, protons, and pions incident on a 4mm Pb/1mm Plastic calorimeter (Histogram -

# Different Neutron Cutoff Times

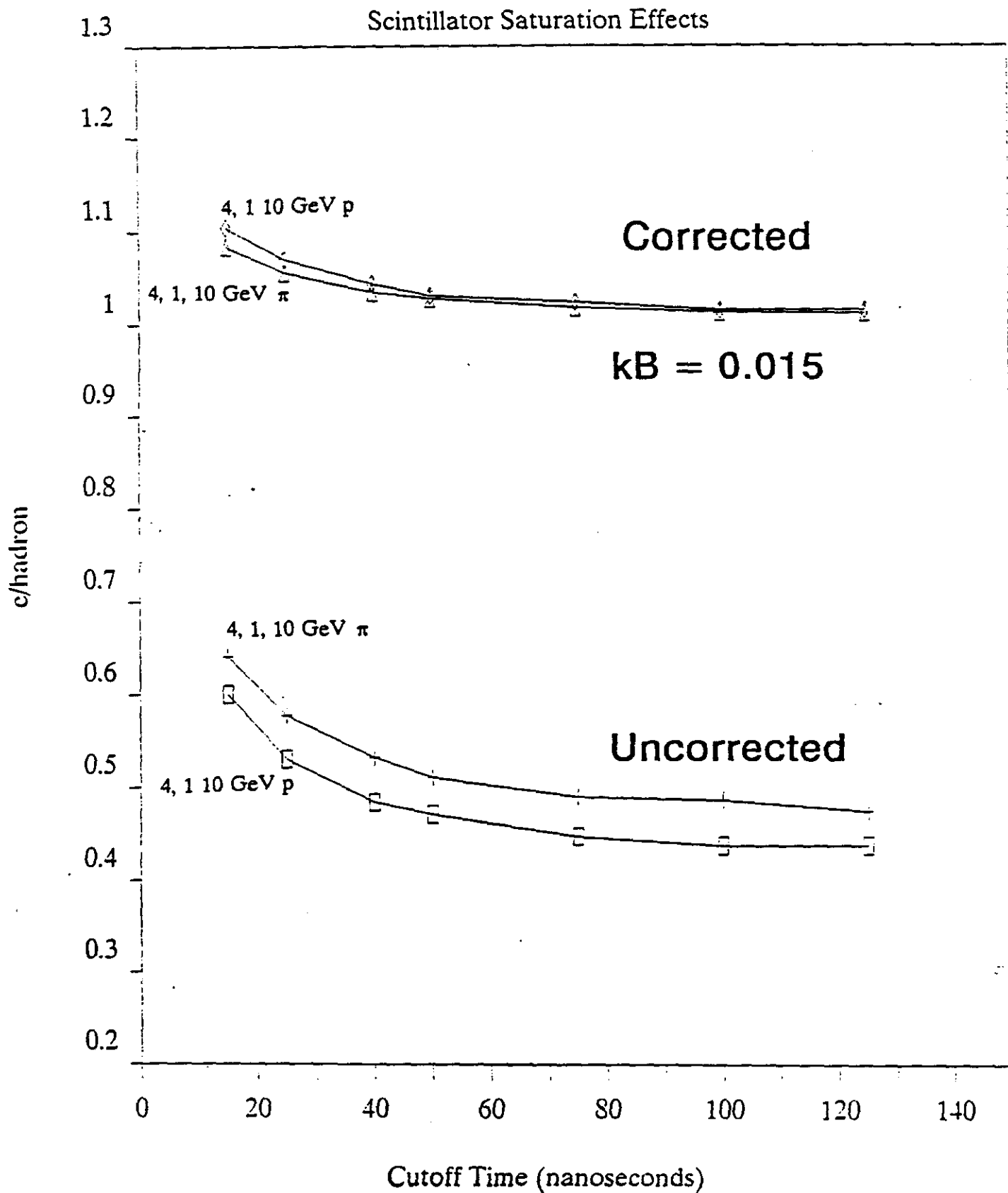
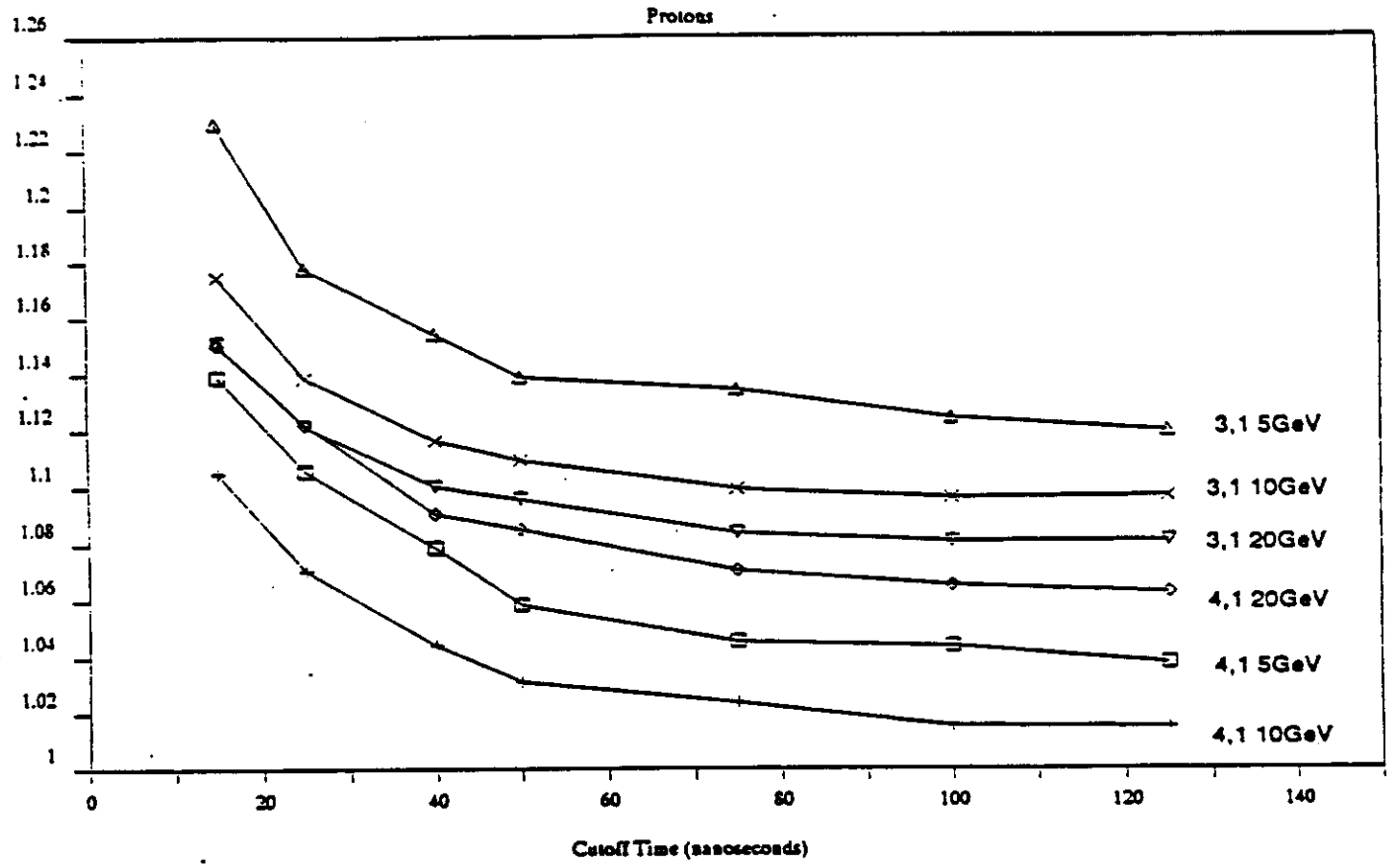


FIG. 3 Variation of compensation as a function of time and saturation level.



Different Neutron Cutoff Times

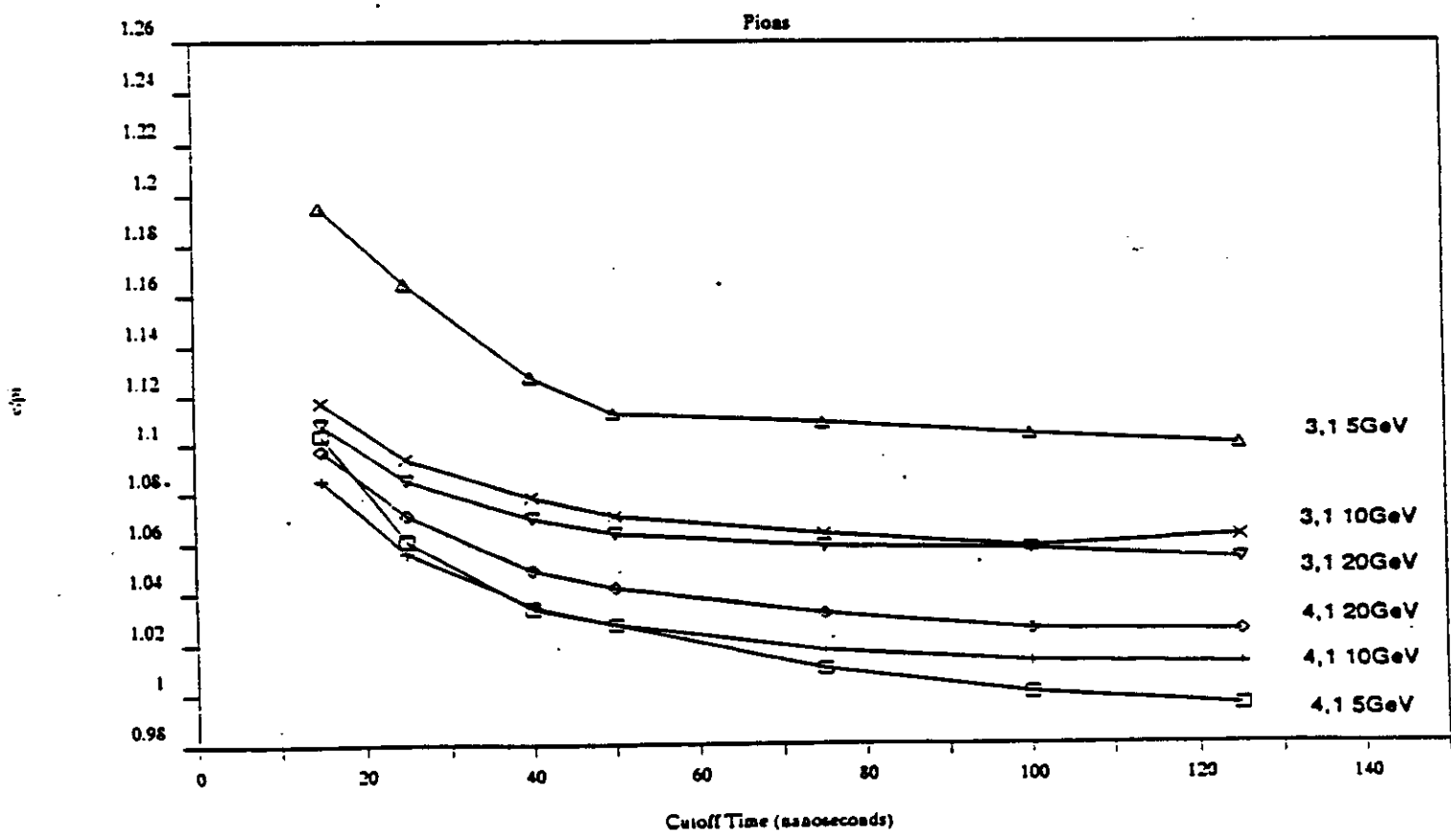
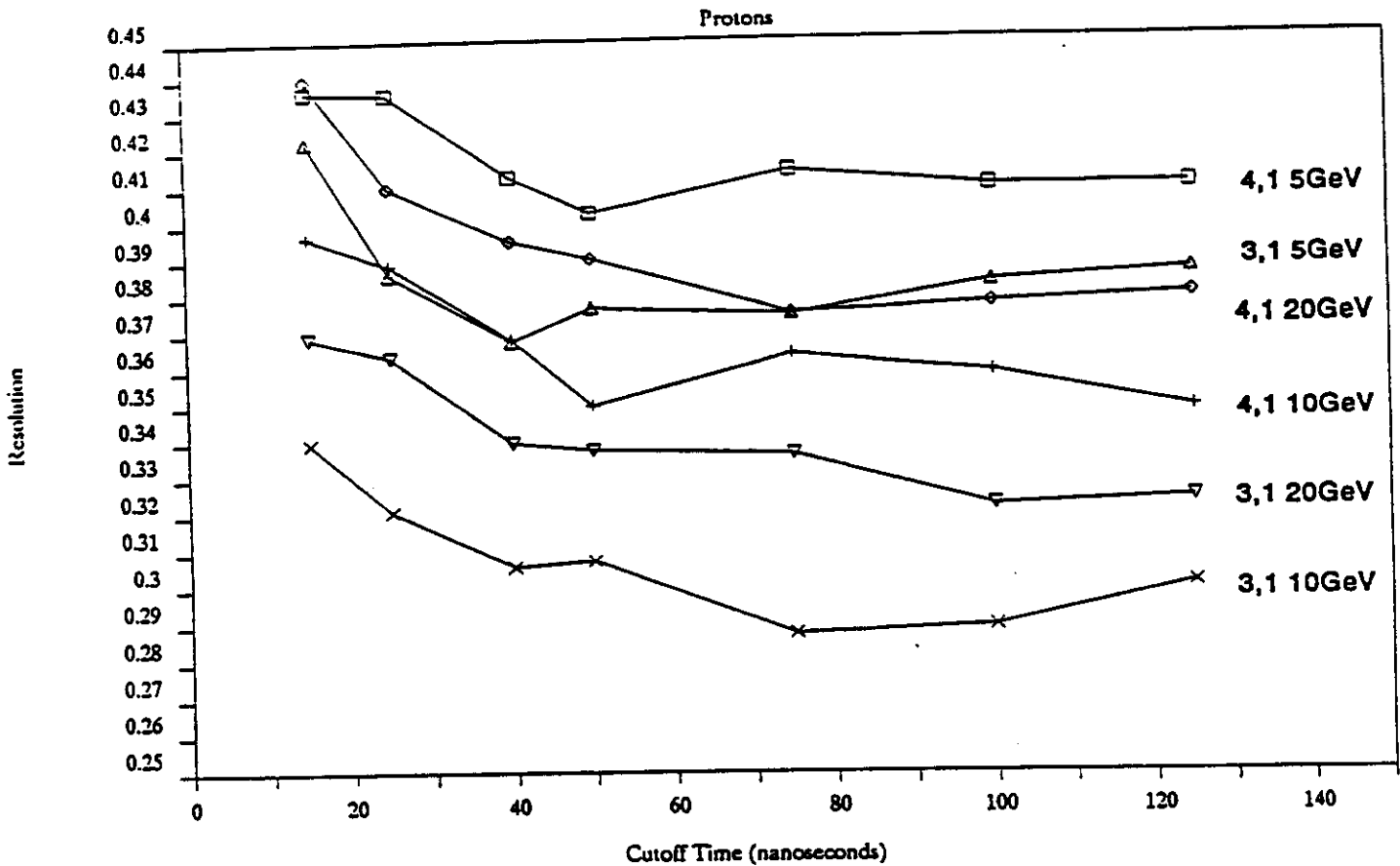


Fig. 4 Variation of compensation as a function of time, energy, and calorimeter geometry.  
 3,1 = 3mm Pb/1mm scintillator  
 4.1 = 4mm Pb/1mm scintillator



Different Neutron Cutoff Times

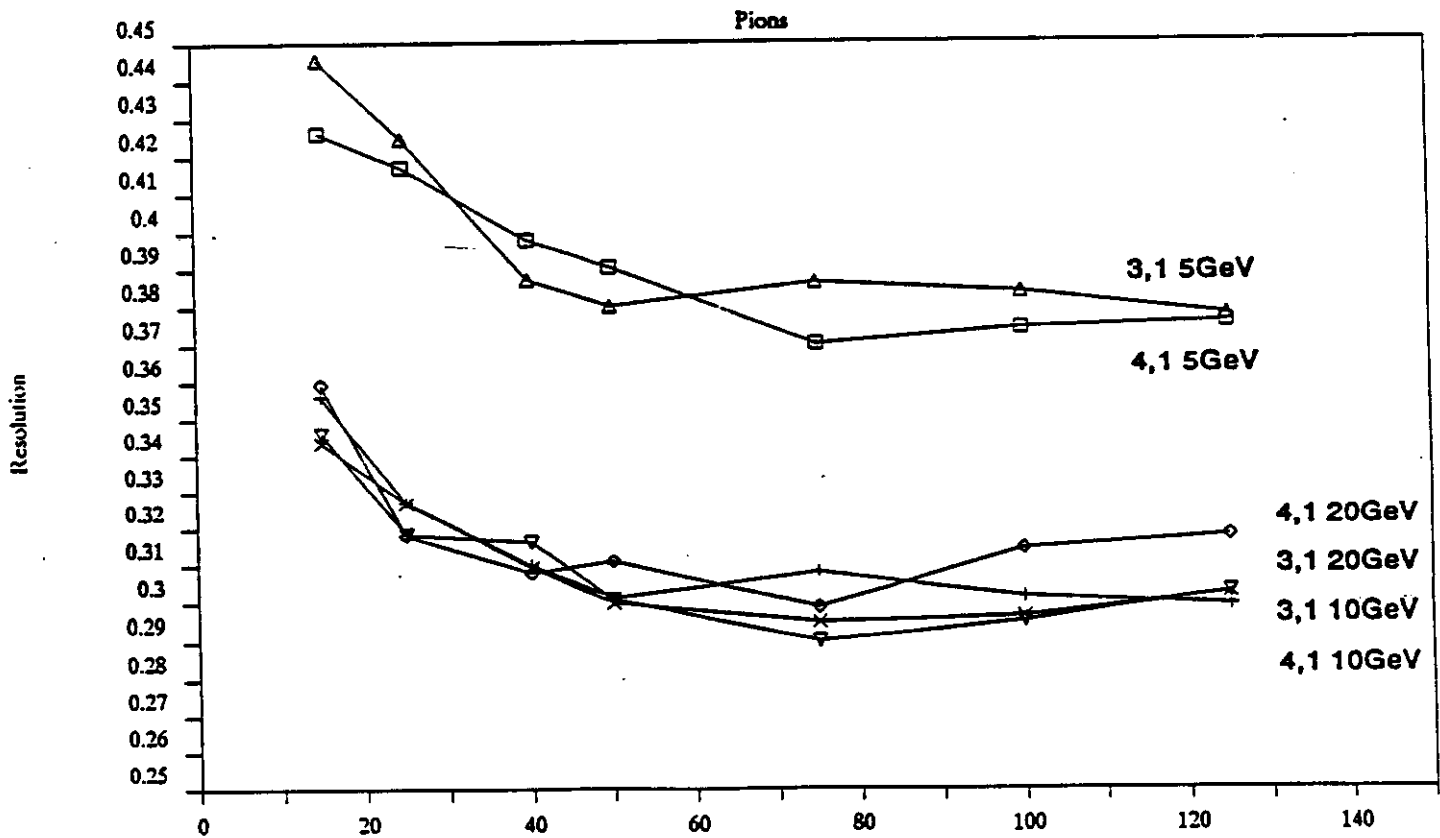


Fig. 5 Variation of resolution ( $\sigma/E = A/\sqrt{E}$ ) as a function of time, energy, and calorimeter.  
 3,1 = 3mm Pb/1mm scintillator  
 4,1 = 4mm Pb/1mm scintillator  
 A is the measure of resolution plotted

#### IV. Radiation Damage Effects on Calorimeter Compensation.

As has been suggested in previous reports and at past conferences, a calorimeter to be used at the Superconducting Super Collider should have an equal response to electromagnetic and hadronic particles, if they are of the same energy. If this is the case, the calorimeter is said to be compensating and the calorimeter considered in this study is of the compensating type. In order to achieve compensation, various combinations of passive and active media have been used. Plastic scintillator in combination with uranium or lead can achieve this desired result.

The detectors at the SSC will have to operate in a hostile radiation environment that has so far not been explored at previous or current accelerators. Therefore, the long-term effects of exposure to radiation are unknown. However, as has been shown at this conference, plastic scintillator does experience a degradation of its output signal when exposed to the radiation doses that are equivalent to what is expected at the SSC<sup>7</sup>. It has also been shown that the signal output of the scintillator does not fully recover with annealing. This implies that the response of the calorimeter will change as a function of time. To determine how the detector response will change is the object of study for this section. The calorimeter configuration used for these studies is the same as the (4,1) used in the previous section, i.e, 4mm Pb/1mm scintillator. This unit cell is repeated 300 times.

This particular configuration of active and passive media turns out to be mildly compensating with  $e/h$  value of 1.05 in the energy range 2 - 20 GeV. To simulate the hadronic and electromagnetic particles entering the SSC calorimeter from 20 TeV p-p collisions, incident 10 GeV negative pions and electrons properly normalized are used.

In the analysis programs, an average energy depth profile was calculated for the pions and the electrons. As can be clearly seen in the unshaded histogram in Fig. 6a, the electrons deposit almost all of their energy in the first 25cm of the calorimeter, whereas the pions (Fig. 6b) more uniformly deposit their energy throughout the calorimeter. From these respective profiles, a combined profile was obtained by adding one-third of the electron signal at a given depth to two-thirds the given pion signal at the same depth. It is assumed that two-thirds of the energy entering the calorimeter at the SSC will be hadronic, while one-third will be electromagnetic. The combined profile is shown in Fig. 6c.

As has been reported by others<sup>7</sup>, the radiation dosage is not uniform in pseudo-rapidity. To take this into account, the plastic scintillator has been degraded by three different dosage rates, 5 Megarads per year, 10 Megarads per year, 15 Megarads per year. These dosages correspond to pseudo-rapidities that are values of 3 and larger. In addition, as has been reported at the Florida State Conference (March, 1990), the degradation factor for plastic scintillator varies depending upon the type of scintillator used. Therefore, the plastic scintillator signal has been degraded by three different values, 0.2% net loss of signal per Megarad per year, 0.5% net loss, and 1.0% net loss.\* The time degradation of the scintillator was carried out in two different ways, 1) a linear loss of signal: effectively, this means that the degradation builds up linearly with time, eventually reaching 100% for one particular case, and 2) a geometric loss signal: this means the resultant signal is a percentage of the previous signal. The first method, of course, is the more severe case.

\*Only the 1.0% data is presented here.

# Electron - 10 Mrad, 5 Years

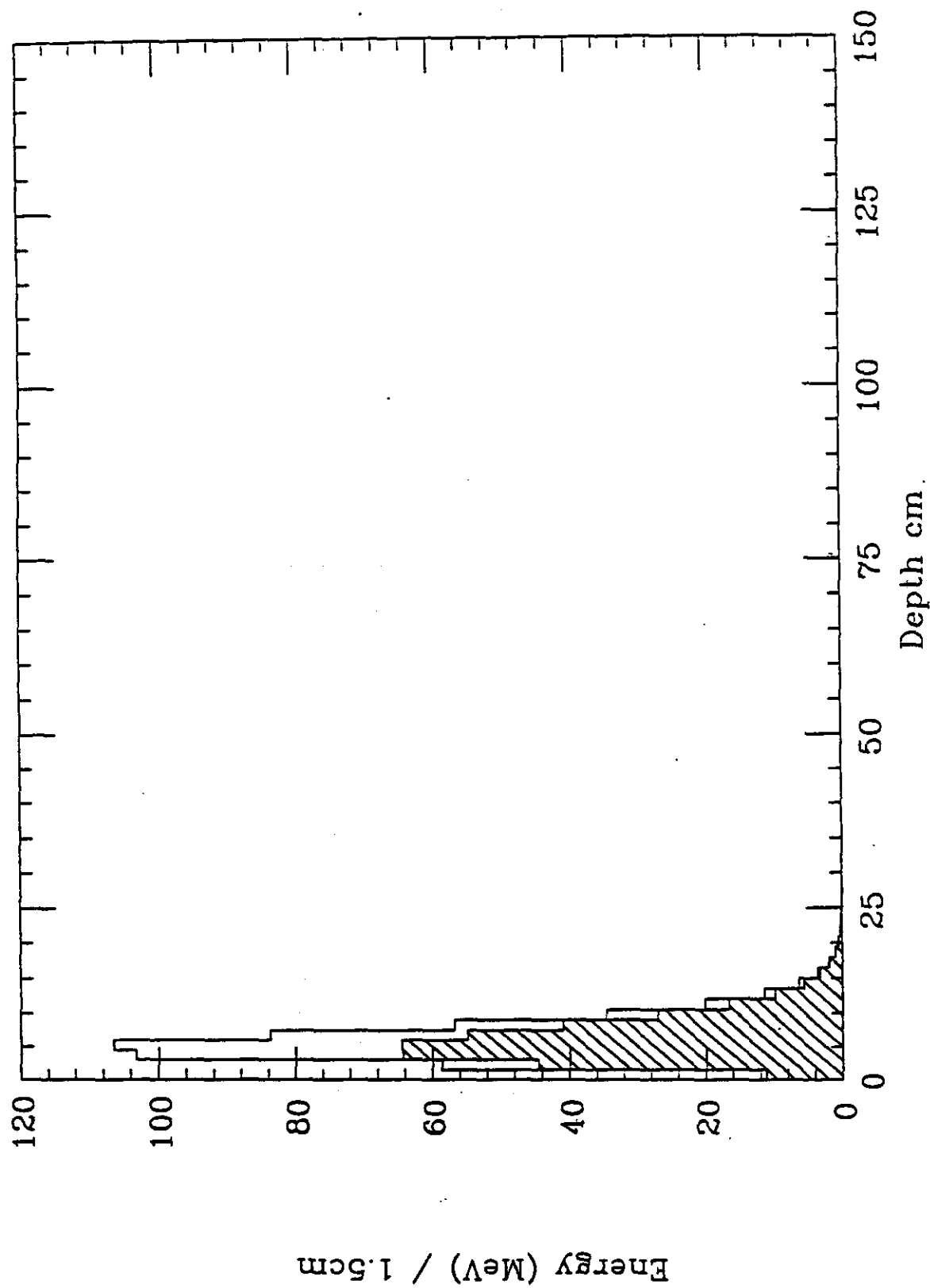


Fig. 6a Electron shower depth profile. The unshaded histogram is the original profile, while the shaded histogram is the resultant profile after 5 years at 10 Mrad/year at 1% signal loss/Megarad/year done geometrically.

# Hadron - 10 Mrad, 5 Years

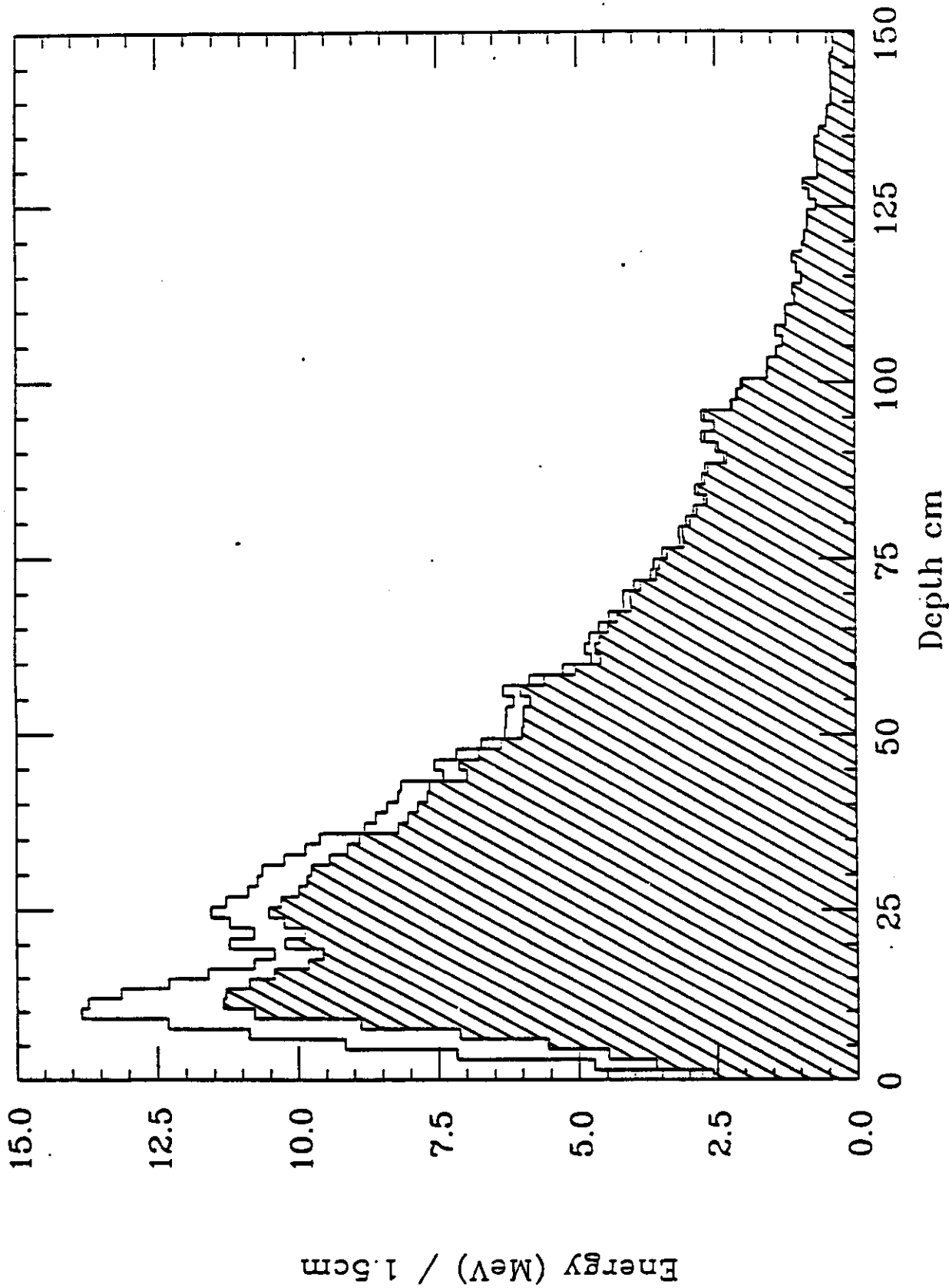


Fig. 6b Hadronic shower depth profile. The unshaded histogram is the original hadronic signal, while the shaded represents the resultant signal after 5 years at 10 Mrad/year at 1% signal loss/Megarad/year.

Combined - 10 Mrad, 5 Years

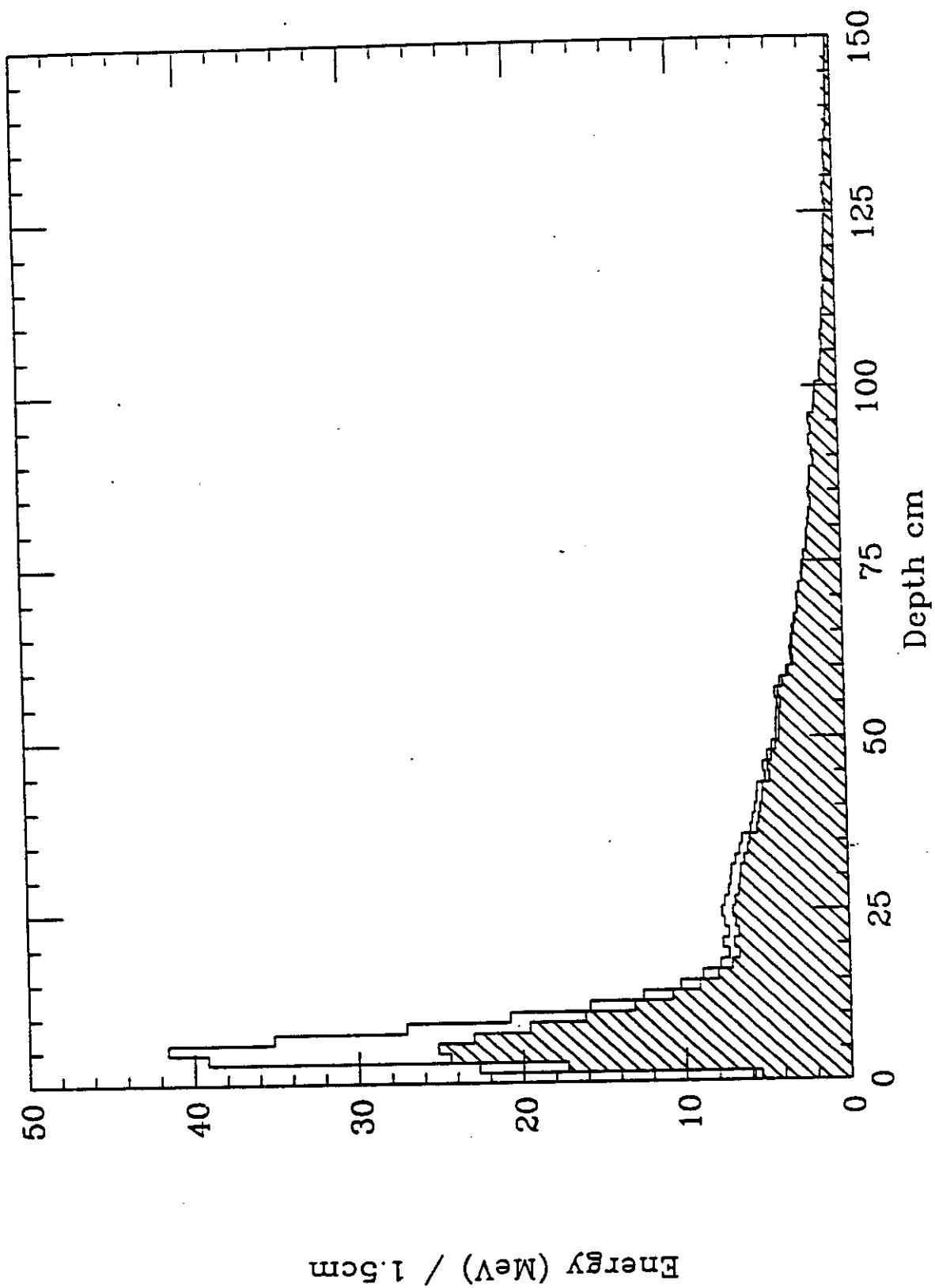


Fig. 6c Similar histograms for the combined signal. The shaded histograms in 6a, 6b and 6c have been done geometrically.

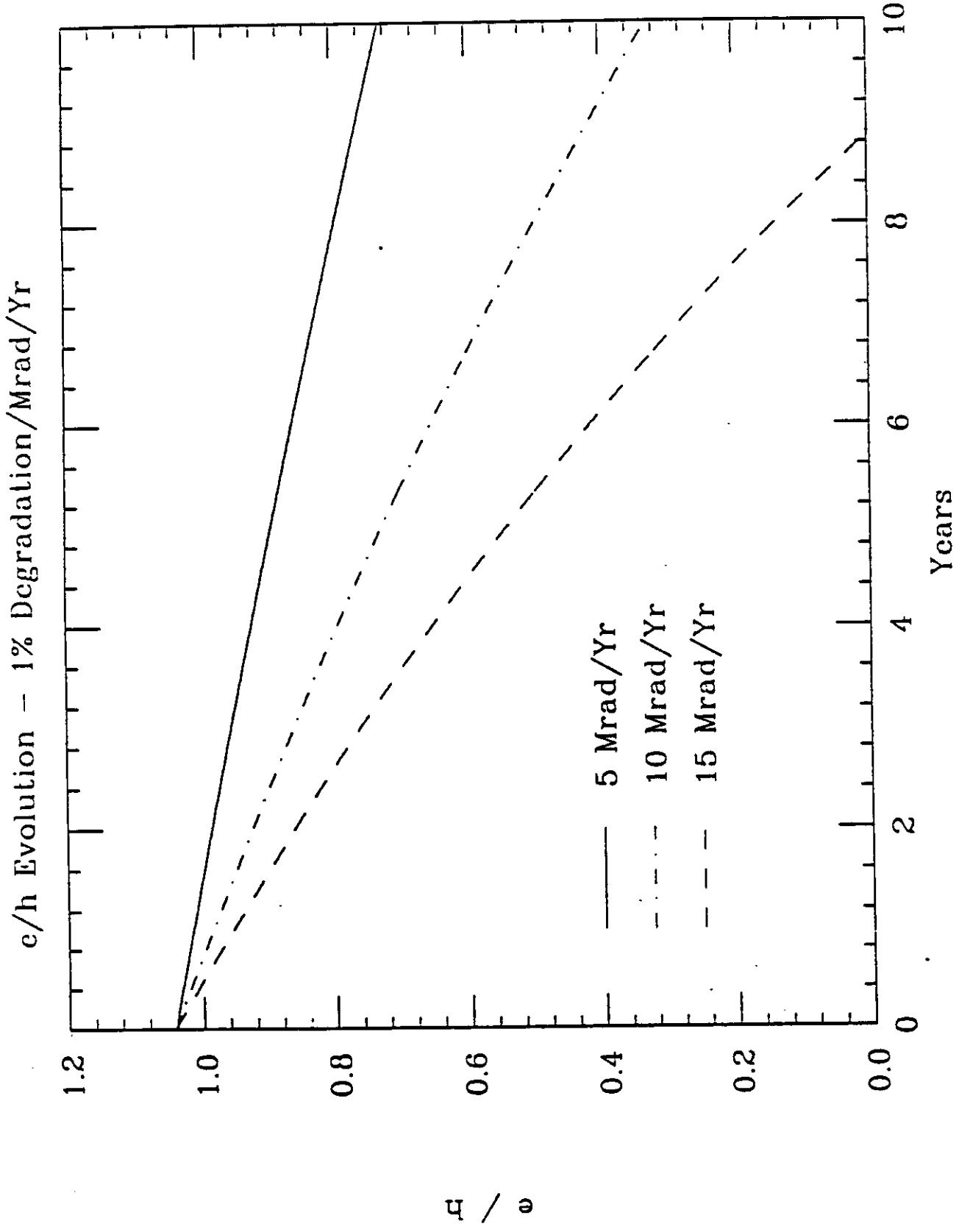


Fig. 7a  $e/h$  evolution for linear degradation.

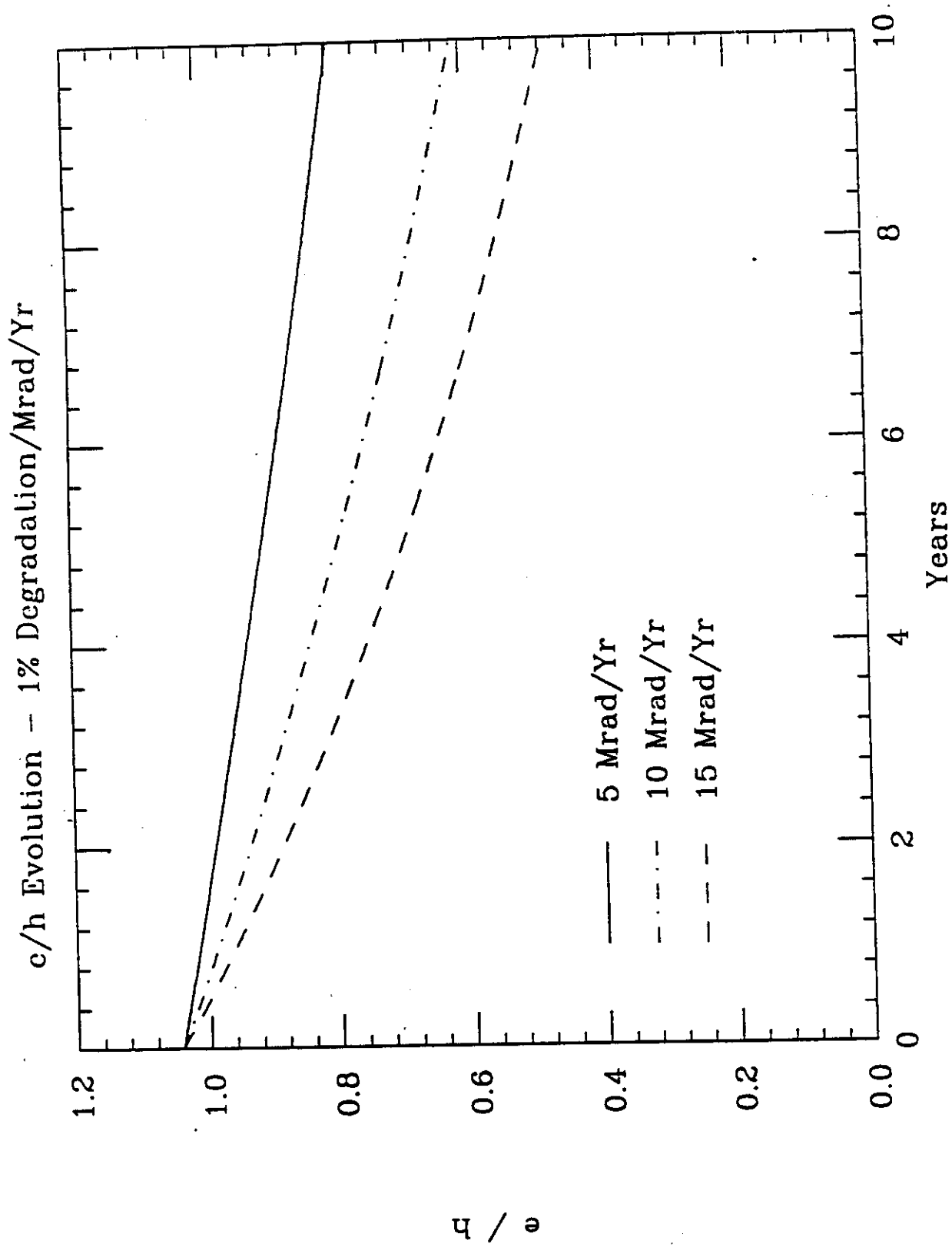


Fig. 7b  $c/h$  evolution for geometric degradation.

The peak of the combined distribution signal corresponds to the maximum dosage per year, and the other bins are accordingly scaled in dosage. The shaded histograms in Fig. 6 represent the resultant signals after an exposure of 10 Megarads per year for 5 years at a degradation factor of 1% done geometrically. As is readily seen, the electron signal is appreciably degraded, whereas the pion signal is hardly affected. This leads to a decrease in the value of  $e/h$  as a function of time.

In Fig. 7a, the  $e/h$  evolution is presented as a function of time for degradation factor of 1% done linearly for the three different dosage rates. As can be seen  $e/h$  rapidly degrades for a dosage rate of 15 Megarads. After a period of two years,  $e/h$  has fallen from an initial value of 1.05 to values of 0.98, 0.92, and 0.86 for the dosage rates of 5, 10, and 15 Megarads, respectively. Therefore, depending on the exact dose rate, the compensation characteristics have decreased by as much as 17% within two years. In Fig. 7b, the  $e/h$  evolution is given for geometric degradation. Here  $e/h$  has fallen to 0.99, 0.93, and 0.88 after two years, again for the same dose rates. Though not as bad as the linear assumption, the geometric case still shows a 15% decrease in compensation due to the plastic scintillator degradation.

As have been shown by the simulation studies, the compensation characteristics of a calorimeter that is part of a detector to be operated at the SSC will be severely degraded as a function of time due to the radiation doses encountered at the SSC. Our estimate that the plastic scintillator will recover to 99% of its signal output is currently over-optimistic. It, therefore, would seem that for a calorimeter to be useful, it will have to have design features that will enable the experimenters to quickly and easily replace the forward sections of the calorimeter, unless sufficiently radiation hardened plastic scintillator becomes available.

## VI General Design Calculations for the SSC Plate Calorimeter

During the Subsystem/CALOR meeting held at ORNL on June 19-20, 1990, several sets of general design calculations to be carried out were agreed upon. This set of calculations will serve two purposes. First of all, a benchmark calorimeter calculation will be carried out at the University of Tennessee, the University of Mississippi, and at Argonne National Laboratory under the auspices of ORNL to ensure that the code system is yielding consistent results. In addition, a series of calculations is planned which will aid in the design of the prototype calorimeter. The following provided by J. Proudfoot outlines the calculations.

### General Discussions

This meeting centered on the material composition issues (scintillator and alloys), EGS parameters, CALOR parameters, and the need for all groups to be using common values, as well as the specific simulation goals. The long-term goal is to study fully a matrix of:

Four scintillator thicknesses (1, 2.5, 5, 10 mm)  
 Four absorber thicknesses (0.5, 1, 2, 4 r.l.)  
 Three primary absorbers (DU, Pb, Fe)  
 Six particle energies (10, 5, 2 GeV)  
 Six integration gate lengths (16, 32, 48, 96, 192, 288 nsec)

### Simulation Parameters

**Geometry:** -1 to 1m in lateral extent  
 8  $\lambda^{1st}$  depth (i.e., excluding plastic)  
 EM section 20 r.l. absorber

**MORSE:**  $t_{max} = 300$  nsec  
 neutron cutoff = 20 MeV  
 ALL OTHERS AT DEFAULT VALUES

**EGS:** Use all default values (No ESTEPE)

**PEGS:**  $e^{\pm}$  cutoff = 1.511 MeV  
 $\gamma$  cutoff = 0.100 MeV

**Remaining Modules:** Use all default values

### Materials Parameters

Scintillator:	C:H	= 0.978
	Density	= 1.04 gm/cm <sup>3</sup>
	Number density H	= 4.92 x 10 <sup>22</sup> atoms/cm <sup>3</sup>
	Number density C	= 4.81 x 10 <sup>22</sup> atoms/cm <sup>3</sup>
	Birk's Constant	= 0.0131 gm/cm <sup>2</sup> /MeV
Depleted Uranium: (100% U <sup>238</sup> )	Density	= 18.95 gm/cm <sup>3</sup>
	$\lambda^{1st}$	= 10.50 cm
	1 r.l.	= 0.33 cm
	Number density	= 4.794 x 10 <sup>-2</sup>
Iron:	Density	= 7.87 gm/cm <sup>3</sup>
	$\lambda^{1st}$	= 16.76 cm
	1 r.l.	= 1.76 cm
	Number density	= 8.486 x 10 <sup>-2</sup>
Lead:	Density	= 11.35 gm/cm <sup>3</sup>
	$\lambda^{1st}$	= 17.09 cm
	1 r.l.	= 0.56 cm
	Number density	= 3.299 x 10 <sup>-2</sup>

## Near-Term Goals and Distribution of Tasks

It was agreed that the time required to complete analysis of the full matrix was substantial, and therefore, achievable near-term goals were established to address the immediate mechanical issues. The analysis is to include the time dependence of shower energy deposition,  $e/h$ , resolution, longitudinal profile and lateral profile.

Runs are to be for:                    10 GeV incident  $e^-$ ,  $\pi^-$   
    1000 histories for  $\pi^-$   
    250 histories for  $e^-$

The three absorbers will be done by separate groups who will each cross check one point for a different absorber. The cross checks, and any additional benchmarks, will be carried out for 2.5mm scintillator and 1 r.l. absorber. The distribution of absorbers is:

<u>Absorber</u>	<u>Group</u>	<u>Cross Check Absorber</u>
Depleted U	University of Tennessee/ORNL	Pb
Pb	Argonne National Laboratory/ORNL	Fe
Fe	University of Mississippi/ORNL	Depleted U

## Configurations

- a) 1 set of points for constant absorber thickness of 1 r.l. at varying scintillator thicknesses of 1mm, 2.5mm, and 10mm.
- b) 1 set of points for a constant scintillator thickness of 2.5mm at varying absorber thicknesses of 0.5, 1, 2, 4 r.l.

## Schedule

- Benchmark configuration run and cross check are to be completed by July 14th.
- Following comparison of results at benchmark configuration, the remaining points are to be run. The target date for completion of this study is September 1, 1990 (optimistic).

## VI ZEUS Benchmark Calculations (as of August 1, 1990)

Due to the need for immediate, preliminary design data and to the late arrival of adequate funding, the ZEUS benchmark calculations are progressing at a slow rate. Currently, the geometry of the prototype calorimeter has been assembled and debugged. Calculations using this geometry with the codes HETC, SPECT (with proper saturation levels), and EGS have been carried out for electrons, protons, and pions at three different energies, 2, 5, and 10 GeV. Only MORSE and the transport of the MORSE produced gamma rays by EGS need to be carried out. Once these final calculations have been done, these data generated by the various codes can be analyzed to determine the calculated responses of the ZEUS prototype calorimeter. Preliminary investigations of the raw data indicate no surprises.